© 2018. Published by The Company of Biologists Ltd | Development (2018) 145, dev162156. doi:10.1242/dev.162156

RESEARCH ARTICLE

Prp8 regulates oncogene-induced hyperplastic growth in *Drosophila*

Cecilia H. Fernández-Espartero[1], Alberto Rizzo[1,*], Alexander D. Fulford[1,*], Julia Falo-Sanjuan[2], Damien Goutte-Gattat[1] and Paulo S. Ribeiro[1,‡]

ABSTRACT

Although developmental signalling pathways control tumourigenic growth, the cellular mechanisms that abnormally proliferating cells rely on are still largely unknown. *Drosophila melanogaster* is a genetically tractable model that is used to study how specific genetic changes confer advantageous tumourigenic traits. Despite recent efforts, the role of deubiquitylating enzymes in cancer is particularly understudied. We performed a *Drosophila in vivo* RNAi screen to identify deubiquitylating enzymes that modulate Ras^{V12}-induced hyperplastic growth. We identified the spliceosome core component Prp8 as a crucial regulator of Ras-, EGFR-, Notch- or RET-driven hyperplasia. Loss of *prp8* function alone decreased cell proliferation, increased cell death, and affected cell differentiation and polarity. In hyperplasia, Prp8 supported tissue overgrowth independently of caspase-dependent cell death. The depletion of *prp8* efficiently blocked Ras-, EGFR- and Notch-driven tumours but, in contrast, enhanced tumours that were driven by oncogenic RET, suggesting a context-specific role in hyperplasia. These data show, for the first time, that Prp8 regulates hyperplasia, and extend recent observations on the potential role of the spliceosome in cancer. Our findings suggest that targeting Prp8 could be beneficial in specific tumour types.

KEY WORDS: Prp8, Tumour growth, *Drosophila*, Spliceosome, Ras

INTRODUCTION

Intensive research in the recent past that has combined molecular profiling approaches with *in vivo* and *in vitro* functional studies has resulted in the identification of genes and pathways that drive tumour formation (Hanahan and Weinberg, 2011). In this regard, the use of the fruit fly *Drosophila melanogaster* as a model organism has been particularly powerful (Gonzalez, 2013; Sonoshita and Cagan, 2017; Tipping and Perrimon, 2014). Indeed, seminal studies using *Drosophila* have led to the identification of multiple genes and signalling pathways, including the Notch (N) and Ras/MAPK pathways that, when mutated, not only cause severe developmental defects but are also involved in tumourigenesis (Gonzalez, 2013). Indeed, different aspects of tumourigenesis have been studied in *Drosophila* and the vast majority of cancer hallmarks are conserved in flies (Hanahan and Weinberg, 2011; Tipping and Perrimon, 2014).

Signalling pathways underpin cellular behaviour and, when disrupted, lead to developmental defects and/or cellular transformation. Virtually all signalling pathways are controlled by post-translational protein modifications, with phosphorylation being the most frequently associated with signalling events (Hynes et al., 2013). However, it is clear that additional post-translational modifications are vital for tightly controlling developmental events. Ubiquitylation, a multi-step cascade that results in the covalent attachment of the small protein ubiquitin onto a substrate, has emerged as a crucial process in signalling that regulates virtually all functions within a cell (Heride et al., 2014). Despite being historically linked with regulation of protein levels and protein degradation, ubiquitylation can also have non-proteolytic effects, leading to changes in protein-protein interactions, protein function and subcellular localisation (Rape, 2017). In a manner akin to phosphorylation, ubiquitylation is reversible, and the removal of ubiquitin moieties from target proteins is controlled by deubiquitylating enzymes (DUBs) (Heride et al., 2014; Rape, 2017). However, the *in vivo* role of DUBs remains poorly explored. This is especially true in the context of developmental and oncogenic growth, despite the fact that many DUBs have recently been linked with tumourigenesis (Fraile et al., 2012).

We performed a *Drosophila in vivo* screening approach to study the role of genes containing domains that are involved in the removal of ubiquitin and ubiquitin-like proteins in the regulation of tumourigenesis. Our top hit was the spliceosome component Prp8, which we identified as a crucial regulator of developmental and hyperplastic growth in several *Drosophila* models of cancer. Prp8 is a core protein of the spliceosome complex and its protein structure includes an MPN/JAB domain typical of the JAMM family of DUBs (Grainger and Beggs, 2005; Komander et al., 2009). Based on sequence and structural analysis, Prp8 is thought to be an inactive DUB, as conserved residues of the JAMM ubiquitin hydrolase domain are absent (Clague et al., 2013; Pena et al., 2007). Nevertheless, the MPN/JAB domain is essential for Prp8 function and can bind ubiquitin with an affinity comparable with that of other ubiquitin-binding domains (Bellare et al., 2006). Our data suggest that Prp8 regulates hyperplasia in a context-dependent manner, which is consistent with previous observations that identified *prp8* as a regulator of organ growth *in vivo*, in a genetic modifier screen that used overexpression of a kinase-dead phosphoinositide 3-kinase (Coelho et al., 2005).

Together with recently published data, our work identifies the spliceosome as a potential target in cancers and suggests that tumours display different sensitivity to disruption of Prp8 function depending on the driver oncogene (Hsu et al., 2015). Thus, our results imply that future therapies that target the spliceosome in

[1]Centre for Tumour Biology, Barts Cancer Institute, Queen Mary University of London, Charterhouse Square, London EC1M 6BQ, UK. [2]Department of Physiology, Development and Neuroscience, University of Cambridge, Downing Street, Cambridge CB2 3DY, UK.
*These authors contributed equally to this work

‡Author for correspondence (p.baptista-ribeiro@qmul.ac.uk)

A.D.F., 0000-0002-8880-1720; P.S.R., 0000-0002-6020-6321

Received 5 December 2017; Accepted 10 October 2018

Development (2018) 145, dev162156. doi:10.1242/dev.162156

cancer may require the identification of the exact context-dependent condition of individual tumours to maximise their efficacy.

RESULTS

In vivo RNAi screening identifies Prp8 as a novel regulator of developmental and oncogene-induced growth

To elucidate the role of DUBs in the regulation of developmental and pathological growth, we performed *in vivo* RNAi screens using lines targeting all *Drosophila* genes that carry a ubiquitin hydrolase domain (Broemer et al., 2010). To explore the role of ubiquitin-related modifications, we also included *Drosophila* orthologues of SUMO and NEDD8 hydrolases in our library of 123 RNAi lines targeting 54 genes (designated herein as DUB^{RNAi} for simplicity) (Table S1). To avoid potential early lethality phenotypes, we regulated RNAi expression spatially and temporally using an *act-Gal4/Gal80^{ts}* module and a *FLP/FRT STOP* cassette (FLPout) (Fig. S1A). We expressed the FLPase enzyme under the control of the eye-specific *eyeless* promoter (*ey-FLP*), such that DUB^{RNAi} expression was limited to the developing eye and was induced by shifting larvae from 18°C to 29°C 120 h after egg laying (AEL) to inhibit *Gal80^{ts}* function.

We initially assessed the role of DUBs in the normal growth of the developing *Drosophila* eye, and identified three genes which, when depleted, caused eye disc hypoplasia: *prp8* (Fig. 1C,G), *usp10* (Fig. S1B) and *npl4* (Fig. S1C). We selected Prp8 for further study as the hypoplasia phenotype was fully penetrant, and was observed in several RNAi lines that target *prp8*, which were predicted to not have off-target effects. We next tested whether DUBs could influence tumour growth. To this end, we co-expressed the DUB^{RNAi} library with an oncogenic form of Ras (Ras^{V12}), thereby mimicking a well-established *Drosophila* tumour model in which expression of Ras^{V12} causes hyperplasia (Lee et al., 1996; Pagliarini and Xu, 2003) (Fig. S1D,L and Table S2). This Ras^{V12} model has been used to identify new regulators of growth and metastasis and, for example, previous research has uncovered the fact that combining Ras^{V12} expression with loss-of-function mutations for polarity genes causes metastasis in larvae (Chabu et al., 2017; Ohsawa et al., 2012; Pagliarini and Xu, 2003). To validate our genetic model, we co-expressed Ras^{V12} with RNAi lines that target the polarity genes *scribbled* ($scrib^{RNAi}$), *lethal giant larvae* (lgl^{RNAi}) and *bazooka* (baz^{RNAi}). Consistent with previous reports, a combination of Ras^{V12} with RNAi against polarity genes resulted in enhanced overgrowth phenotypes in eye discs and, in some cases, in the appearance of distant metastases (compare Fig. S1D with Fig. S1E-G). Therefore, our model mimicked previously used systems to study oncogene-mediated growth and metastasis, and is an appropriate setting to test the role of DUBs in these processes.

Analysis of Ras^{V12}-expressing eye discs with simultaneous depletion of *prp8* (Fig. 1D,H) revealed a dramatic reduction of eye disc overgrowth and a partial rescue of disc morphology when compared with Ras^{V12} expression alone (Fig. 1B,F). Indeed, the major effect of *prp8* depletion in Ras^{V12} tumours was a decrease in size, such that the GFP-positive area in developing eye discs appeared to be similar to that of the controls (compare Fig. 1E with H, quantified in Fig. S4K). When analysed collectively, $prp8^{RNAi}$ lines led to decreased hyperplastic growth in ∼80% of cases, with some of these eye discs displaying a near rescue of eye disc morphology (∼25% of cases) (Fig. 1I and Fig. S1L). In ∼20% of eye discs we still observed tumours and, in rare cases (8.5%), *prp8* depletion in Ras^{V12} tumours caused metastases to appear in developing larvae (Fig. S1L). For the majority of our experiments, we used a $prp8^{RNAi}$ line that resulted in a higher frequency of complete rescue of Ras^{V12}-induced hyperplasia ($prp8^{RNAi\ 18567GD}$). Importantly, although we detected a significant percentage of tumours in whole larvae when this RNAi line was combined with Ras^{V12}, upon eye disc dissection in subsequent experiments, the vast majority of Ras^{V12}; $prp8^{RNAi}$ tissues were significantly smaller than Ras^{V12}-expressing tissues, suggesting that our analysis of intact larvae in fact overestimates the existing tumour growth. We confirmed the effect of *prp8* using the MARCM system to combine loss-of-function of *prp8* ($prp8^{KG03188}$) with expression of Ras^{V12}. Our experiments revealed that, as in the $prp8^{RNAi}$, *prp8* loss-of-function clones are smaller than control clones

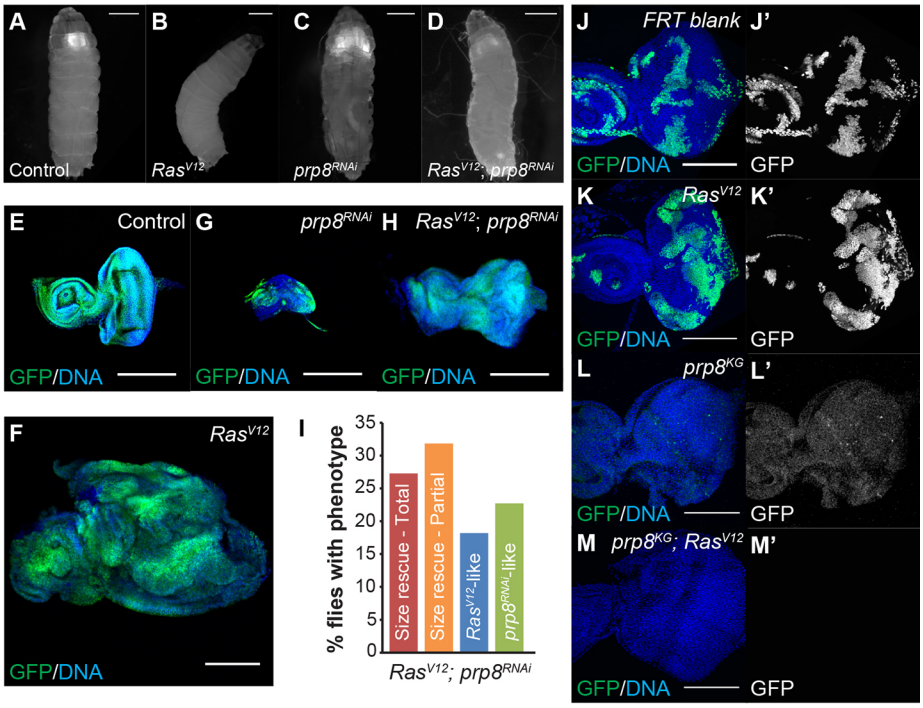

Fig. 1. *prp8* knockdown regulates growth during development and tumourigenesis. (A-D) Images of third instar larvae showing distribution of GFP expression induced in the eye discs and optic lobes of control (A), Ras^{V12} (B), $prp8^{RNAi}$ (C) and Ras^{V12}; $prp8^{RNAi}$ (D). (E-H) Confocal micrographs of eye imaginal discs from third instar larvae of the indicated genotypes, stained with anti-GFP (green) and the DNA marker Hoechst (blue). When compared with controls (A and E), $prp8^{RNAi}$ decreased the GFP-positive area in whole larvae (C) and caused eye disc hypoplasia (G). When combined with Ras^{V12} expression, *prp8* depletion led to a decrease in the GFP-positive area (D) and partially rescued eye disc morphology (H), when compared with Ras^{V12} alone (B and F). (I) Quantification of frequency of phenotypes observed with all $prp8^{RNAi}$ lines used in this study (n>60). (J-M) *xy* sections of third instar eye discs containing clones that were induced with the MARCM system. MARCM *FRT42D* blank clones (J), *UAS-*Ras^{V12} MARCM clones (K), $prp8^{KG03188}$ MARCM clones (L) and $prp8^{KG03188}$; *UAS-*Ras^{V12} MARCM clones (M) are marked by GFP (green). DNA is stained with Hoechst (blue). Scale bars: 1 mm in A-D; 200 µm in E-H; 100 µm in J-M.

Development (2018) 145, dev162156. doi:10.1242/dev.162156

(compare Fig. 1J with 1L). Moreover, combining Ras^{V12} with *prp8* loss-of-function resulted in a phenotype similar to *prp8* loss alone (compare Fig. 1M with 1L). Together, our results suggest that Prp8 influences Ras^{V12}-mediated hyperplastic growth and that, to a large extent, depletion of *prp8* impairs Ras^{V12}-mediated hyperplasia.

Prp8 controls cell proliferation and cell death

To elucidate how Prp8 regulates tissue growth, we tested whether the eye disc hypoplasia phenotype obtained with depletion of Prp8 was because of cell proliferation defects. For this, we assessed the levels of phosphohistone-H3 (PH3), a marker of cells that are undergoing mitosis. When compared with controls (Fig. 2A), $prp8^{RNAi}$ discs displayed reduced cell proliferation (Fig. 2C, quantified in Fig. 2I). In contrast, the number of PH3-positive cells seen in discs that expressed Ras^{V12} (Fig. 2B) or the Ras^{V12}; $prp8^{RNAi}$ combination (Fig. 2D) was similar to controls (Fig. 2A, quantified in Fig. 2I). We also analysed the G2/M cyclin, Cyclin B (CycB) (Fig. S2A-D) and found that, in both Ras^{V12} and $prp8^{RNAi}$ samples, CycB distribution was altered. CycB levels in the presumptive second mitotic wave were reduced in Ras^{V12}-expressing cells (Fig. S2B), whereas in $prp8^{RNAi}$ the sharp boundary of CycB expression was lost and its expression was more uniform throughout the disc (Fig. S2C). In both cases, the morphogenetic furrow is absent. Interestingly, depleting *prp8* in Ras^{V12}-expressing cells leads to a partial rescue of the CycB phenotype and the appearance of a rudimentary morphogenetic furrow (Fig. S2D). We also analysed the number of cells entering S phase by assessing 5-bromo-2′-deoxyuridine (BrdU) incorporation (Fig. S2E) and found that, as expected, Ras^{V12} increased the number of BrdU-positive cells, which was suppressed when combined with $prp8^{RNAi}$. These results suggest that the eye phenotypes that are associated with *prp8* depletion may be due to cell proliferation defects, which is consistent with a previous report that stated *prp8* depletion causes a G2/M arrest (Andersen and Tapon, 2008). Depleting *prp8* from Ras^{V12}-expressing tissues reduced entry into S phase but not progression through mitosis, as there was no significant difference in the number of PH3-positive cells between Ras^{V12} and Ras^{V12}; $prp8^{RNAi}$ tissues. Therefore, the effect of Prp8 on cell proliferation appears to be insufficient to explain why the loss of Prp8 blocks Ras^{V12}-induced hyperplasia.

These observations raise the possibility that Prp8 may affect cell survival. We assessed this using an antibody that recognises cleaved caspases (anti-Dcp1 antibody) and, therefore, reflects the overall level of cell death. Control eye discs have a relatively low level of cell death, which is mostly restricted to the area that juxtapose the morphogenetic furrow (Fig. 2E, quantified in Fig. 2J) (Rusconi et al., 2000). Expression of Ras^{V12} alone did not significantly alter cell death levels (Fig. 2F,J). In contrast, $prp8^{RNAi}$ led to a dramatic increase in caspase staining (Fig. 2G,J). Combining Ras^{V12} with *prp8* depletion resulted in a significant decrease in the levels of active caspase compared with $prp8^{RNAi}$ alone, which suggests that

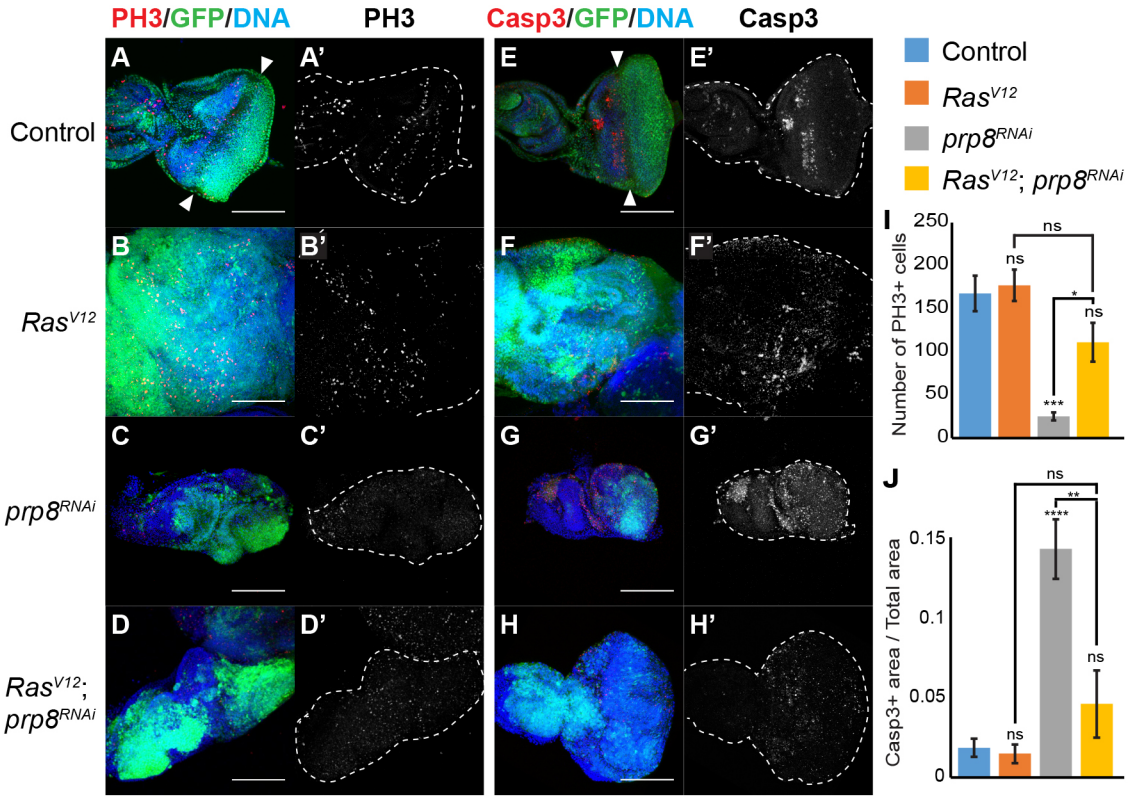

Fig. 2. Prp8 modulates eye disc development by controlling cell proliferation and cell death. (A-H) Confocal micrographs of eye imaginal discs of the indicated genotypes, labelled with anti-GFP (green), Hoechst (blue) and either anti-phospho Histone H3 (PH3) (A-D, red) or anti-cleaved Caspase 3 (Dcp1) (E-H, red). (I) Quantification of number of PH3-positive cells in eye discs (n>5 discs/genotype). (J) Quantification of the ratio between Caspase 3-positive area and total eye disc area (n>6 discs/genotype). PH3 was mainly detected adjacent to the morphogenetic furrow (arrowheads) in controls (A and A′). In Ras^{V12}-expressing discs, the PH3 pattern was mislocalised (B,B′). *prp8* knockdown resulted in fewer PH3-positive cells (C,C′ and I), whereas combining Ras^{V12} with $prp8^{RNAi}$ resulted in an intermediate phenotype (D,D′ and I). $prp8^{RNAi}$ increased cell death (G,G′ and J), which was partially rescued by co-expression with Ras^{V12} (H,H′ and J). Dashed outlines indicate the outline of the eye disc. Data are mean±s.e.m. *P<0.05; **P<0.01; ***P<0.001; ****P<0.0001 (one-way ANOVA analysis). ns, non-significant. Scale bars: 100 µm.

Development (2018) 145, dev162156. doi:10.1242/dev.162156

Ras^{V12} can rescue the cell autonomous defects that lead to cell death when *prp8* is depleted (Fig. 2H,J). Nevertheless, depletion of *prp8* in Ras^{V12} tumours resulted in reduced hyperplastic growth (Fig. 2H). Together, these results suggest that loss of Prp8 function leads to defects in eye disc morphology due to a combination of decreased proliferation and increased cell death. However, when oncogenic Ras is present, Prp8 blocks hyperplasia, despite only having a modest effect on cell proliferation and cell death levels relative to Ras^{V12} alone. To confirm that cell death alone cannot explain the phenotypes associated with loss of Prp8, we used the caspase inhibitor P35. Expression of *P35* in controls did not result in any overt changes in tissue size or number of GFP-positive cells in developing eye discs (Fig. S2F). Consistent with our hypothesis, co-expression of $prp8^{RNAi}$ and *P35* was insufficient to fully rescue the hypoplasia phenotype that was seen when *prp8* was lost, despite reducing the levels of activated caspases (compare Fig. S2G with Fig. 2G, quantified in Fig. S2H). Therefore, we conclude that although cell death contributes to the $prp8^{RNAi}$ phenotype, there appear to be other processes that are regulated simultaneously (including cell proliferation) that contribute to regulation of developmental and Ras^{V12}-induced hyperplastic growth.

Prp8 regulates cell differentiation in the developing *Drosophila* eye

We next assessed whether Prp8 could regulate other processes that influence eye disc development. We first tested cell differentiation, as Prp8 has been associated with differentiation defects (Keightley et al., 2013; Wu et al., 2016) and, in *Drosophila*, eye disc development involves close coupling of cell proliferation, death and differentiation (Cagan, 2009). Moreover, crucial eye disc determinants are thought to be regulated via alternative splicing events (Fic et al., 2007; Roignant and Treisman, 2010), a process for which Prp8 function is crucial (Grainger and Beggs, 2005). To assess whether Prp8 regulates cell differentiation in eye discs, we stained for the photoreceptor differentiation marker Embryonic lethal abnormal vision (Elav, an RNA-binding protein that acts as a neuronal marker), the transcription factor Reversed polarity (Repo, which is restricted to glial cells) and the transcriptional co-activator Eyes absent (Eya, expressed in progenitors before differentiation) (Bonini et al., 1993; Lee and Jones, 2005; Soller and White, 2004). In controls, Elav and Repo were detected primarily in the region posterior to the morphogenetic furrow, which determines the 'front' of the cell differentiation wave (Fig. 3A,E). In $prp8^{RNAi}$ discs, Elav staining was completely lost (Fig. 3C). Repo staining was still detectable in *prp8*-depleted discs, but the localisation and morphology of Repo-positive cells was dramatically changed (Fig. 3G). In contrast, whereas some Ras^{V12}-expressing cells maintained Elav and Repo expression, the majority were negative for these differentiation markers and, therefore, are presumably undifferentiated (Fig. 3B,F). Interestingly, when Ras^{V12} was combined with $prp8^{RNAi}$, both Elav and Repo were expressed in the overgrown tissue and, when compared with Ras^{V12} alone, these tissues appeared to have a higher percentage of Elav-positive and Repo-positive cells and resembled the control situation (Fig. 3D,H, quantified in 3M). With regard to Eya, its expression pattern was disrupted in Ras^{V12}- (Fig. 3J) and $prp8^{RNAi}$-expressing tissues (Fig. 3K), compared with controls (Fig. 3I) but, contrary to Elav and Repo, this was not rescued in the Ras^{V12}; $prp8^{RNAi}$ combination (Fig. 3L), indicating that the effect of *prp8* may be limited to specific differentiation markers.

We also assessed whether *prp8* depletion affected signalling downstream of Ras^{V12}, as it has been previously reported that

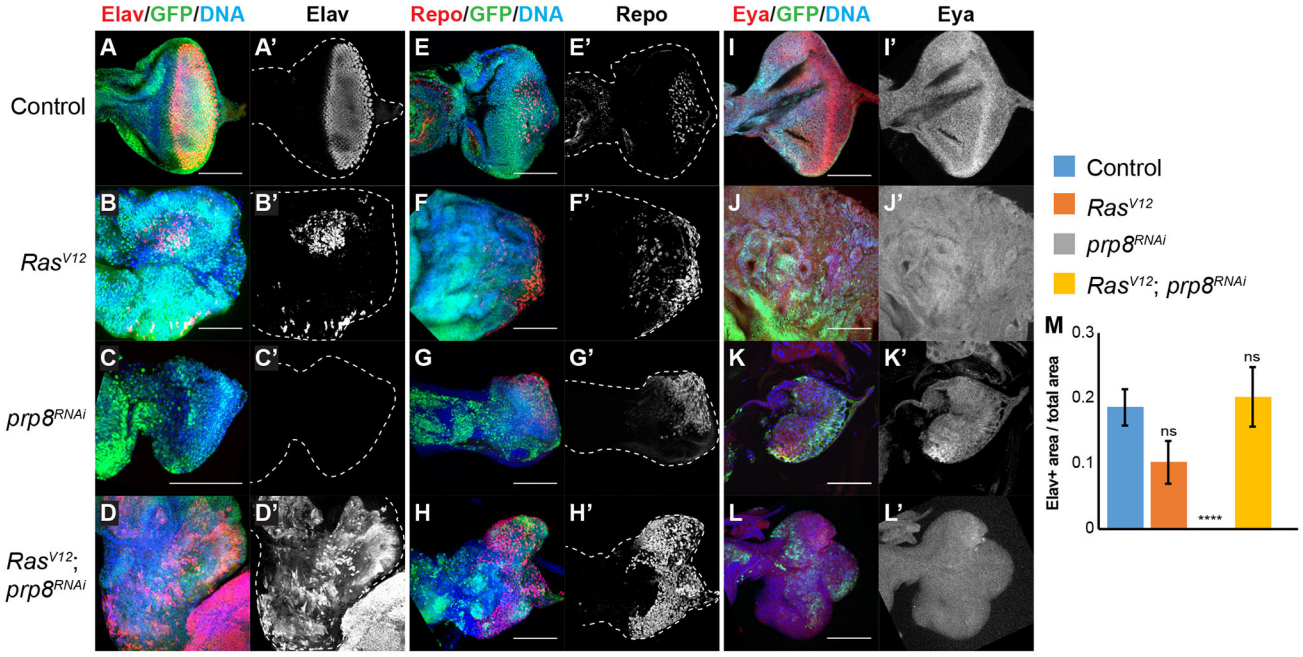

Fig. 3. *prp8* depletion induces cell differentiation in hyperplastic tumours. (A-L) Confocal micrographs of eye imaginal discs of the indicated genotypes, labelled with anti-GFP (green), Hoechst (blue) and either anti-Elav (A-D, red), anti-Repo (E-H, red) or anti-Eya (I-L, red). Both Elav and Repo are located in the posterior region of control eye discs (A,A′ and E,E′). Ras^{V12} inhibited differentiation to a large extent (B,B′ and F,F′). $prp8^{RNAi}$ discs lost Elav expression (C,C′), whereas Repo staining remained largely unaffected (G,G′). Co-expression of Ras^{V12} and $prp8^{RNAi}$ resulted in an increase in the number of Elav (D,D′) or Repo (H,H′) positive cells, when compared with Ras^{V12} alone. The pattern of Eya expression in controls (I,I′) is severely disrupted in Ras^{V12} (J,J′) or $prp8^{RNAi}$ (K,K′) discs. (M) Quantification of the ratio between Elav-positive area and total eye disc area (n>4 discs/genotype). Dashed outlines indicate the outline of the eye disc. Data are mean±s.e.m. ****P<0.0001 (one-way ANOVA analysis). ns, non-significant. Scale bars: 100 µm.

Development (2018) 145, dev162156. doi:10.1242/dev.162156

alterations in spliceosome genes cause dramatic changes in the splicing pattern of MAPK (Ashton-Beaucage et al., 2014). We analysed total and phospho-MAPK levels *in vivo* (Fig. S3A-J) and splicing changes in S2 cells (Fig. S3K and L) and found minor changes, under the conditions tested. Accordingly, expression of MAPK (*rolled*; *rl*) in $prp8^{RNAi}$-expressing tissues was unable to rescue $prp8^{RNAi}$-mediated hypoplasia, despite the fact that the eye disc morphology was partially rescued (Fig. S3M-P). Therefore, it is unlikely that the effect of *prp8* in Ras^{V12} hyperplasia is due to an effect on MAPK regulation.

Our data suggest that Prp8 can regulate cell differentiation in developing eye discs and that, in the presence of oncogenic Ras, absence of Prp8 function prevents uncontrolled growth, not by affecting MAPK signalling downstream of Ras but, at least in part, by causing premature or enhanced differentiation of cells. This would render the cells postmitotic, thereby limiting the growth of Ras^{V12} hyperplastic tissues.

Prp8 regulates oncogenic tissue morphology in part by affecting cell polarity

Our data suggest that $prp8^{RNAi}$ can partially rescue the overall morphology of Ras^{V12} hyperplastic eye discs (Fig. 1). Therefore, we hypothesised that Prp8 regulates cell processes and the components that are crucial for establishing and/or maintaining tissue morphology, such as polarity and the actin cytoskeleton (Pickup et al., 2002). To address this, we performed immunofluorescence staining for F-actin and the polarity protein Discs large (Dlg) in developing eye discs (Fig. 4). F-actin has a stereotypical organisation, with a prominent accumulation in the morphogenetic furrow and at the periphery of the posterior region of the disc (Fig. 4A). In Ras^{V12} discs, the loss of overall tissue organisation and structure is reflected in the localisation of F-actin. F-actin is abnormally accumulated in large patches, which are adjacent to regions in which total F-actin appears to be significantly downregulated (Fig. 4B). Surprisingly, $prp8^{RNAi}$-associated eye disc hypoplasia was not accompanied by prominent changes in F-actin organisation beside an interruption of the F-actin signal in lateral membranes (Fig. 4C). In *prp8*-depleted eye discs, F-actin still accumulates at the periphery of the posterior region of the disc (Fig. 4C). When Ras^{V12} and $prp8^{RNAi}$ were combined (Fig. 4D), we observed that, despite a significant rescue of overall tissue morphology and tissue size, the F-actin pattern was still disorganised and did not resemble either wild-type (Fig. 4A) or $prp8^{RNAi}$ phenotypes (Fig. 4C). Our results suggest that Prp8-mediated regulation of hyperplasia is mostly independent of a potential minor role of Prp8 in the modulation of the actin cytoskeleton. This hypothesis is consistent with our observation that F-actin structure is still disorganised when *prp8* is depleted from Ras^{V12}-expressing hyperplastic tissue.

We next examined whether modulation of cell polarity could explain the rescue of tissue morphology that was seen when $prp8^{RNAi}$ was combined with Ras^{V12}. Dlg is a basolateral polarity determinant that localises to septate junctions and is visualised in the lateral side of cells (Fig. 4E). Expression of Ras^{V12} results in Dlg mislocalisation, which appears to spread throughout the cell membrane (Fig. 4F). Loss of *prp8* leads to a dramatic increase in Dlg levels, loss of apico-basal polarity and epithelial organisation (Fig. 4G). When combined with Ras^{V12}, $prp8^{RNAi}$ partially rescued Dlg localisation, which is more lateral than in Ras^{V12} tumours alone, recapitulating the situation seen in the controls (compare Fig. 4H with Fig. 4E and Dlg localisation in cross-section images). Collectively, these results indicate that Prp8 regulates levels and/or localisation of Dlg and this modulation of cell polarity function may be, at least in part, responsible for the rescue of tissue morphology seen during hyperplasia.

Prp8-mediated regulation of oncogenic growth is not tissue-specific

Next, we determined whether the effect of Prp8 in the regulation of oncogene-induced hyperplasia was a tissue-specific function or

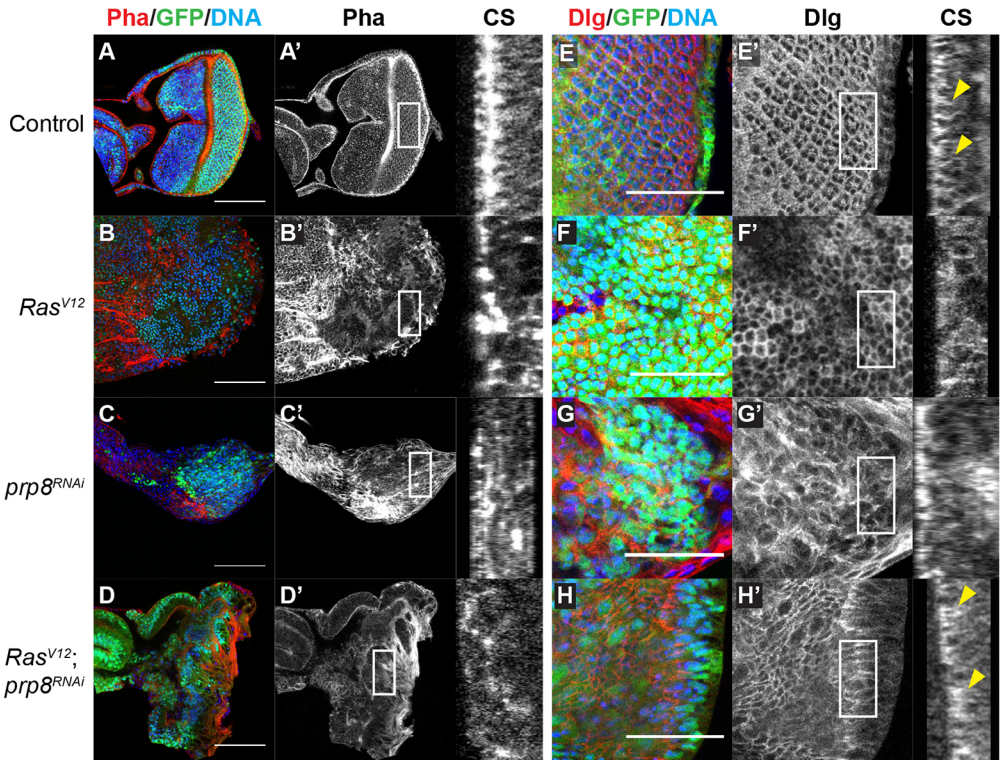

Fig. 4. *prp8* regulates cell polarity but not actin localisation in Ras^{V12}-induced hyperplasia. (A-D) Confocal micrographs depicting eye disc morphology for the indicated genotypes. Eye disc morphology was assessed by staining F-actin using rhodamine-conjugated phalloidin (Pha, red). Ras^{V12} expression caused severe morphology defects and disruption of the F-actin pattern (B,B′). $prp8^{RNAi}$ induced eye disc hypoplasia and F-actin mislocalisation (C,C′), which persisted when combined with Ras^{V12} (D,D′). (E-H) Confocal micrographs of eye discs of the indicated genotypes stained for anti-Dlg (red). Ras^{V12} expression caused spreading of Dlg to the entire cell perimeter (F,F′). Whereas $prp8^{RNAi}$ alone resulted in Dlg mislocalisation (G,G′), combined expression with Ras^{V12} rescued the localisation of Dlg (H,H′). CS denotes cross-section images (indicated by boxed areas in A′-H′). Yellow arrowheads denote regions in which the Dlg pattern is similar in controls and Ras^{V12}; $prp8^{RNAi}$ tissues. Scale bars: 100 µm in A-D; 40 µm in E-H.

Development (2018) 145, dev162156. doi:10.1242/dev.162156

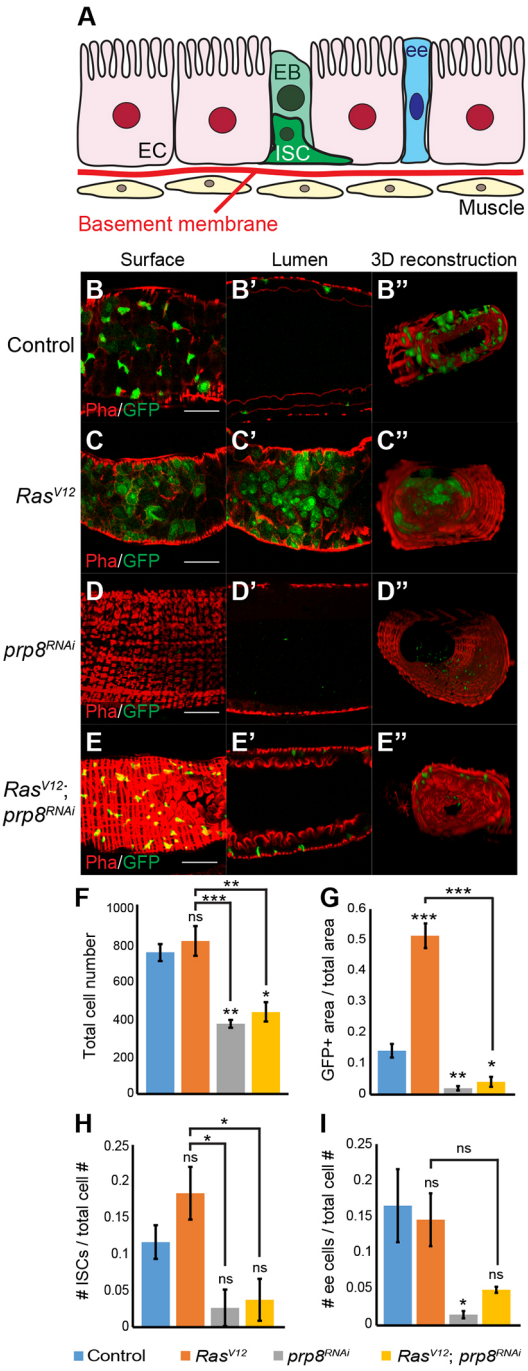

Fig. 5. Prp8 regulates intestinal stem cell dynamics and prevents Ras-induced hyperplasia in the adult gut. (A) Schematic of adult gut structure, including the different cell types present: intestinal stem cells (ISC), enteroblasts (EB), enteroendocrine cells (EE), enterocytes (EC) and the underlying basement membrane and muscle layer. (B-E) Confocal micrographs of posterior midguts from adult flies of the indicated genotypes, stained for GFP (green) and F-actin (phalloidin, Pha, red). Shown are surface plane images (B-E), lumen sections (B′-E′) and 3D reconstructions (B′′-E′′) of the posterior midgut region. (F) Quantification of total number of cells in the posterior midgut, 7 days after induction (n>9 guts/genotype). (G) Quantification of the ratio between the GFP-positive area and total area of the posterior midgut, 7 days after induction (n>12 guts/genotype). (H) Quantification of the ratio between the number of Delta-positive (Dl, ISC marker) cells and total number of cells in the posterior midgut, 7 days after induction (n>4 guts/genotype). (I) Quantification of the ratio between the number of enteroendocrine cells [Prospero (Pros)-positive] and total number of cells in the posterior midgut, 7 days after induction (n>6 guts/genotype). Data are mean±s.e.m. *P<0.05; **P<0.01; ***P<0.001 (one-way ANOVA analysis). ns, non-significant. Scale bars: 50 µm. For B″-E″, the images represent an area of 206.18 µm^2.

whether it was limited to the regulation of Ras^{V12}-induced hyperplasia. For this, we generated alternative hyperplasia models in the developing eye using activated versions of the EGF receptor ($Egfr^{\lambda top}$) and Notch ($N^{\Delta ECD}$) (Pallavi et al., 2012; Queenan et al., 1997) (Fig. S4). Similar to Ras^{V12}, expression of EGFR (Fig. S4A) or N (Fig. S4C) led to overgrowth phenotypes. *prp8* depletion significantly reduced the hyperplasia caused by both genes and, in some cases, produced a dramatic rescue of tissue organisation (Fig. S4B,D). Significantly, this suggests that *prp8* regulates hyperplastic growth that is induced by different oncogenes. Moreover, we tested whether the effect of *prp8* on Ras^{V12}-induced hyperplastic growth was a general role for the spliceosome by depleting the expression of alternative spliceosome components, such as Mfap1 (part of the spliceosome complex B; Fig. S4E,F), Prp38 (part of complex B; Fig. S4G,H) and Bx42 (part of complexes B, C and P; Fig. S4I,J). We found that all the spliceosome components efficiently suppressed Ras^{V12}-induced hyperplasia in the eye, suggesting that, at least in this tissue, the effect of *prp8* is likely to be mediated by its role in the spliceosome (Fig. S4E-J, quantified in Fig. S4K).

We also assessed whether Prp8 regulated Ras^{V12}-induced hyperplasia in other tissues. To test this, we selected the adult gut as a model, as expression of Ras^{V12} in intestinal stem cells (ISC) is known to cause tissue hyperplasia (Ragab et al., 2011; Jiang et al., 2011). The adult gut is maintained by ISCs, which can be identified by the expression of the N ligand Delta (Dl) and small nuclear size. ISCs give rise to enteroblasts (EB) that can differentiate into either enteroendocrine cells (ee) or absorptive enterocytes (EC) (Fig. 5A). Both ISCs and EBs express the transcription factor gene *escargot* (*esg*) and, in our experiments, we combined *esg-Gal4* with a temperature-sensitive version of *Gal80* to control gene expression (Fig. 5A) (Micchelli and Perrimon, 2006; Ohlstein and Spradling, 2006). When compared with controls (Fig. 5B), *esg-Gal4*-mediated expression of Ras^{V12} in the adult gut led to an increase in the relative area of GFP-positive cells (ISCs and EBs) in the posterior midgut, 7 days after induction (Fig. 5C, quantified in 5G). The total cell number (Fig. 5F) and, in relative terms, the number of GFP-positive cells were similar to controls (Fig. S5I), which suggests that most of the GFP-positive area is because of large GFP-positive cells, which are likely to be ECs in which GFP expression now persists or progenitor cells that become enlarged. Accordingly, the number of small GFP-positive cells (ISCs and/or progenitors) is similar to control (Fig. S5J). Ras^{V12}-mediated hyperplasia influenced tissue architecture and, in some cases, caused GFP-positive cells to invade the gut lumen (Fig. 5C). In contrast, *prp8* depletion resulted in a significant reduction in GFP-positive area (Fig. 5D,G), accompanied by a significant reduction in the relative number of GFP-positive cells (Fig. S5I). Similar to what we observed in the developing eye, co-expression of Ras^{V12} and $prp8^{RNAi}$ resulted in a significant reduction in the levels of Ras^{V12}-induced hyperplasia (Fig. 5E,G and Fig. S5I), which suggests that Prp8 influences Ras^{V12}-mediated growth in different tissues.

Next, we assessed whether *prp8* depletion also affected cell proliferation, differentiation and death in the adult gut. Therefore, we stained adult guts with the ISC marker Dl (Fig. 5H and Fig. S5A-D), the ee marker Prospero (Pros) (Fig. 5I and Fig. S5E-H) and an antibody against active caspases (Fig. 6 and Fig. S6).

Development (2018) 145, dev162156. doi:10.1242/dev.162156

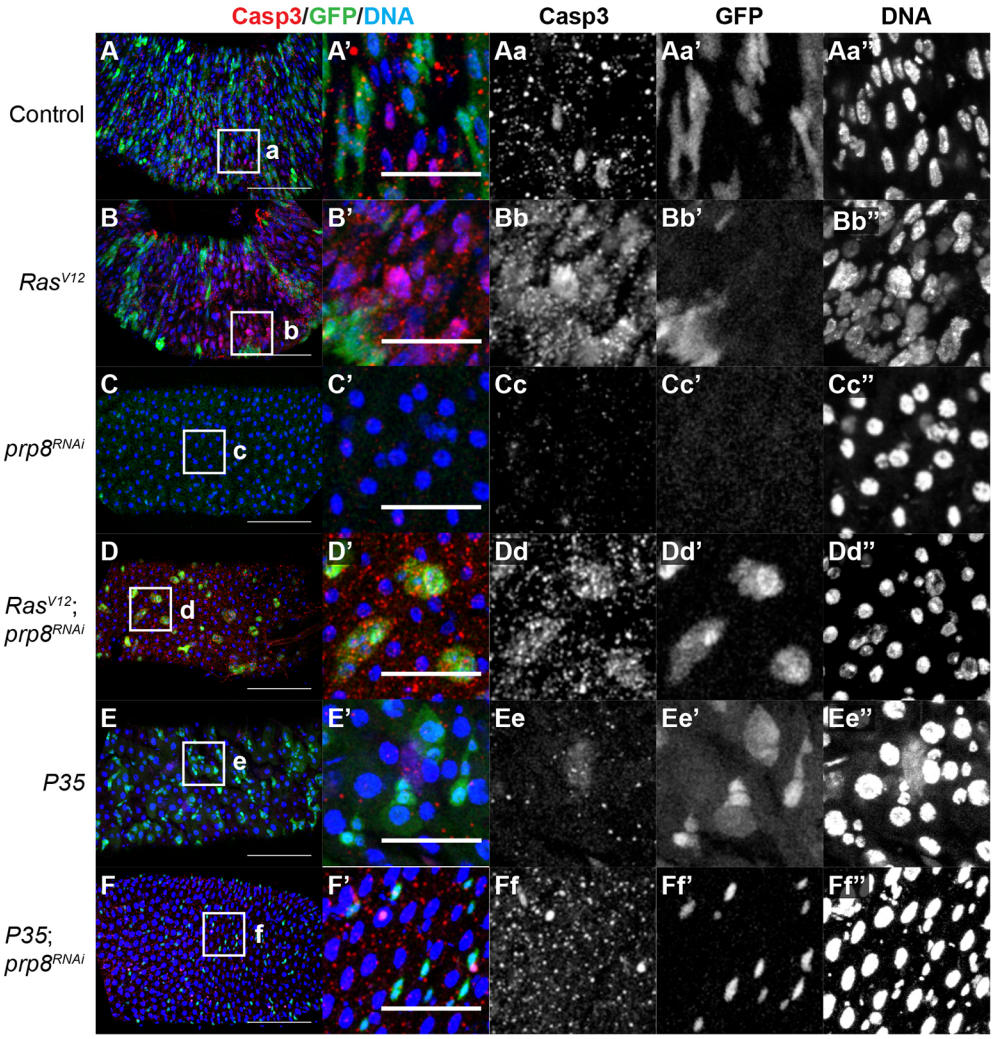

Fig. 6. Blocking caspase activity is not sufficient to restore ISC levels in *prp8^{RNAi}* adult guts. (A-F) Confocal micrographs of posterior midguts from adult flies of the indicated genotypes, stained for cleaved Caspase 3 (Casp3; red in A-F, grey in Aa-Ff), GFP (green in A-F, grey in Aa′-Ff′) and DNA (blue in A-F, grey in Aa′′-Ff′′) 2 days after induction of gene expression. Boxed areas (a-f) indicate regions of interest shown in magnified images (Aa-Ff). Note that P35 reduced Casp3 levels (E) but this did not abrogate the effect of *prp8^{RNAi}* on the number of ISCs (F). Scale bars: 100 µm in posterior midgut images A-F; 40 µm in magnified images A′-Ff′′.

Expression of *Ras^{V12}* did not significantly change the ratio of Dl-positive cells in the gut, which suggests that although *Ras^{V12}* promotes the proliferation of ISCs or uncommitted progenitors, these are likely still differentiating appropriately (Fig. 5H and Fig. S5B). In contrast, *prp8^{RNAi}*, alone or in combination with *Ras^{V12}*, led to a significant decrease in the ratio of Dl-positive cells relative to *Ras^{V12}* alone, suggesting that it blocks *Ras^{V12}* hyperplasia by blocking ISC and/or progenitor proliferation, promoting their differentiation or inducing apoptosis (Fig. 5H, Fig. S5C,D). With regard to ee cells, *Ras^{V12}* expression had no effect on the proportion of ee cells in the adult gut, which suggests that the increased proliferation of ISCs and/or progenitors does not result in increased levels of differentiation to the ee lineage (Fig. 5I and Fig. S5F). In contrast, the proportion of ee cells was markedly reduced in *prp8^{RNAi}*-expressing guts (Fig. 5I, Fig. S5G and H). As the proportion of ee cells decreased when Prp8 was absent, these results suggest that it is unlikely that Prp8 loss blocks *Ras^{V12}* tumours by promoting the differentiation of ee cells.

Finally, we analysed the levels of activated caspases in the posterior midgut at different times after gene induction to determine whether modulation of caspase-dependent cell death could explain the phenotypes that are seen with *prp8^{RNAi}* alone or in combination with *Ras^{V12}*. In controls (Fig. S6A), the levels of apoptosis 4 days after induction were low and the majority of caspase-positive cells were GFP-negative (therefore not *esg-Gal4* positive), which is in agreement with the fact that most of the remodelling in the gut happens at the level of ECs and ee cells (Amcheslavsky et al., 2009; Jiang et al., 2009). In guts that expressed *Ras^{V12}*, there was an increase in the number of caspase-positive cells, which were found both in areas that contained GFP-positive cells and in adjacent GFP-negative areas (Fig. S6B). This suggests that *Ras^{V12}* increases cell proliferation but also cell death, both in ISCs/progenitors and GFP-negative cells. This would explain why the total number of cells in the posterior midgut was similar between controls and *Ras^{V12}* (Fig. 5F). When we depleted *prp8* using the *esg-Gal4* driver, we observed very low levels of caspase staining 4 days after induction (Fig. S6C). This was also the case when *prp8* was depleted in combination with *Ras^{V12}* expression (Fig. S6D). At later stages (7 days after transgene induction), the number of caspase-positive cells was low in all genotypes (data not shown). Therefore, we assessed an earlier time point, 2 days after induction, which yielded similar results (Fig. 6A-D). However, in this situation we observed caspase activity in GFP-positive cells of *Ras^{V12}; prp8^{RNAi}* animals, which indicated a potential loss of progenitor cells (Fig. 6D). In addition, we tested whether blocking apoptosis using P35 could rescue the reduction in the number of GFP-positive cells that was seen when *prp8* was depleted. Expression of *P35* alone reduced active caspase levels but had no overt effect on the adult gut 2 days after induction (Fig. 6E). Flies that expressed *prp8^{RNAi}* and *P35* displayed phenotypes that were similar to *prp8^{RNAi}* alone (compare

Development (2018) 145, dev162156. doi:10.1242/dev.162156

Fig. 6C with F), which indicates that blocking cell death is insufficient to rescue the *prp8*^{RNAi} phenotype. These results suggest that either Prp8 does not affect cell death in these conditions or that cell death occurs at an earlier time point and/or is caspase-independent. Depleting *prp8* in the context of *Ras*^{V12} hyperplasia was associated with cell death, but it was not overtly different from the caspase activation that was seen in *Ras*^{V12}-expressing tissues. Together, our data suggest that Prp8 reduces *Ras*^{V12}-mediated hyperplastic growth in different tissues, potentially using context-dependent tissue-specific mechanisms (i.e. modulation of proliferation and differentiation in the eye versus modulation of proliferation in the gut).

Prp8 antagonises RET-induced cell invasion

Next, we tested whether Prp8 regulates oncogene-induced hyperplastic growth and invasion in the developing wing disc. For this, we combined *prp8*^{RNAi} with expression of an oncogenic version of the receptor tyrosine kinase RET (*RET*^{MEN2B}; M955T point mutation) in the anterior-posterior boundary of the developing wing disc using *patched-Gal4* (*ptc-Gal4*), as this system has previously been used to study invasion and metastasis and the receptor tyrosine kinase RET (Das et al., 2013; Read et al., 2005; Rudrapatna et al., 2012). Activating mutations in RET lead to the cancer syndrome multiple endocrine neoplasia type 2, which is associated with the occurrence of multiple tumours, including the highly metastatic medullary thyroid carcinoma. RET was used in this instance as *ptc-Gal4*-mediated expression of *Ras*^{V12} led to early lethality, even when crosses were performed at 18°C (data not shown). As previously shown, when compared with controls (Fig. 7A), expression of oncogenic RET increased the *ptc-Gal4*-expressing area (Fig. 7B, quantified in Fig. 7E) (Das et al., 2013). In contrast, *prp8* depletion resulted in disruption of the wing morphology and the appearance of GFP-positive cells outside of the *ptc* domain, indicative of potential cell invasion, which is in sharp contrast to what we observed in the eye disc and adult gut in the presence of oncogenic Ras (Fig. 7C,E). This phenotype was significantly enhanced when *prp8* depletion was combined with RET expression, with a clear increase in the number of GFP-positive cells outside of the *ptc-Gal4* domain (Fig. 7D,E). These results suggest that, in this tissue, *prp8* may act as a tumour suppressor gene. Alternatively, the distinct outcome that is seen when removing *prp8* function in both settings could be due to the activation of different signalling modules by *Ras*^{V12} or oncogenic RET, that is, the function of Prp8 would be context-dependent. We also assessed the levels of caspase activation in this setting and found that both control (Fig. S7A) and RET-expressing wing discs exhibited low levels of caspase activation (Fig. S7B). In agreement with our eye disc data, depletion of *prp8* led to moderate caspase activation in the *ptc*-expressing domain, which is consistent with previous reports (Fig. S7C) (Claudius et al., 2014). Surprisingly, when *prp8*^{RNAi} was combined with RET expression, the levels of caspase activation were dramatically increased, particularly in areas that were adjacent to wild-type cells (Fig. S7D). This suggests that the increased invasion of *prp8*^{RNAi}; *RET*^{MEN2B} cells may be driven by an increase in caspase activity. This hypothesis is in line with previous studies that implicate caspases in cell invasion via the activation of JNK signalling and subsequent activation of matrix metalloproteases that remodel the extracellular matrix and destroy the basement membrane, allowing cells to invade (Rudrapatna et al., 2013). We also assessed whether the effect of Prp8 in RET-induced hyperplasia could be a general feature of affecting spliceosome function. We depleted *mfap1* (Fig. S7E,F), *prp38* (Fig. S7G,H) or

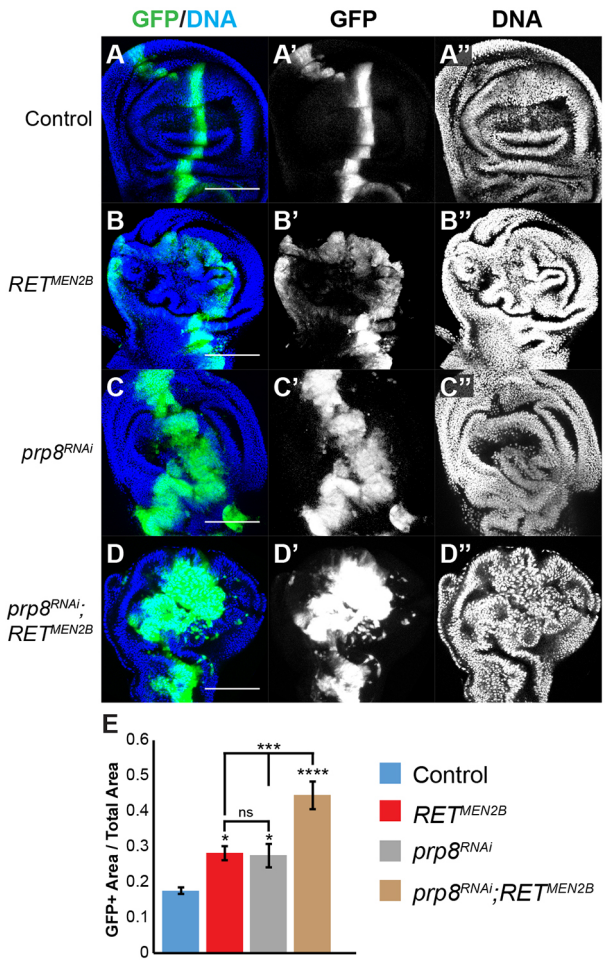

Fig. 7. Loss of *prp8* enhances the proliferation and invasion phenotype of oncogenic RET. (A-D) Confocal micrographs of wing imaginal discs from third instar larvae of the indicated genotypes, stained for GFP (green) and DNA (blue). GFP expression marks the anterior-posterior boundary and the *ptc-Gal4*-expressing domain. *RET*^{MEN2B} expression (B) and *prp8* depletion (*prp8*^{RNAi}; C) caused an increase in the GFP-positive area, when compared with controls (A). Combining *RET*^{MEN2B} and *prp8*^{RNAi} enhanced the *RET*^{MEN2B} phenotype and the appearance of invasive cells outside the anterior-posterior boundary (D). (E) Quantification of the ratio between the GFP-positive area and total area of the wing disc in the indicated genotypes (n>7 discs/genotype). Data are mean±s.e.m. *P<0.05; ***P<0.001; ****P<0.0001 (one-way ANOVA analysis). ns, non-significant. Scale bars: 100 µm.

bx42 (Fig. S7I and J) in the *ptc-Gal4* domain and found that, in marked contrast to *prp8* depletion, removing the function of these spliceosome components significantly suppressed the *RET*^{MEN2B} phenotype (compare Fig. S7F,H,J with Fig. S7B). Collectively, our results identify Prp8 as a crucial regulator of hyperplastic growth. The precise function of Prp8 in tumours still requires further studies but appears to depend on the driving oncogene and may involve tissue-specific mechanisms, which may be dependent or independent of the function of Prp8 in the spliceosome.

DISCUSSION

In this report, using an *in vivo* RNAi screening approach, we identify Prp8 as a crucial regulator of oncogene-induced hyperplastic growth in *Drosophila*. Depletion of *prp8* in the developing eye caused significant hypoplasia, suggesting that Prp8 is required for eye disc development. Depleting *prp8* in *Ras*^{V12}-expressing tissues suppressed the *Ras*^{V12} overgrowth phenotype and, in some cases, resulted in a

Development (2018) 145, dev162156. doi:10.1242/dev.162156

rescue of the global tissue structure. Despite the fact that $prp8^{RNAi}$ tissues display increased apoptosis and reduced proliferation, this alone is unlikely to account for all of the phenotypes that were observed when *prp8* was depleted alone or in combination with Ras^{V12}. Indeed, simply blocking apoptosis in *prp8*-depleted tissues was insufficient to rescue the eye disc hypoplasia phenotype. This suggests that Prp8 has a complex pleiotropic effect during development and in the context of deregulated growth, in line with its role as a crucial spliceosome component (Grainger and Beggs, 2005; Shi, 2017). Accordingly, in tissues that express both Ras^{V12} and $prp8^{RNAi}$, hyperplasia was decreased, despite the fact that apoptosis levels were significantly reduced compared with $prp8^{RNAi}$ alone. Moreover, the levels of proliferation were not significantly affected. This raises an important question: how does *prp8* depletion suppress hyperplasia in the absence of changes in proliferation and caspase-dependent cell death? One possible explanation is the apparent increase in cell differentiation that is seen in Ras^{V12}; $prp8^{RNAi}$ tissues, which would preclude further proliferation, as cells would enter a postmitotic state (Silies et al., 2010). This is a potentially conserved strategy, as there are examples of differentiation acting as a tumour-suppressive mechanism in mammals, most notably in relation to p53 function and Notch signalling in skin cancer (Bieging et al., 2014; Guinea-Viniegra et al., 2012; Restivo et al., 2011). In several *Drosophila* tissues, Ras^{V12} expression blocks differentiation, at least in part, by co-opting JNK activity (Brumby et al., 2011; Pastor-Pareja and Xu, 2013; Zeng et al., 2010). Loss of *prp8* function in this context may affect the ability of Ras to block differentiation programs. Indeed, depletion of *prp8* alone led to changes in cell differentiation in the eye disc and a specific loss of neuronal markers. Interestingly, a zygotic Prp8 mutant in zebrafish displayed extensive neuronal cell loss, as well as defects in the differentiation of myeloid cells (Keightley et al., 2013). This observation, combined with the suggestion that genes that are essential for eye disc development undergo alternative splicing, suggests that Prp8 has a conserved function in the regulation of developing neurons and is involved in cell fate decisions (Fic et al., 2007; Keightley et al., 2013; Roignant and Treisman, 2010). Alternatively, depletion of *prp8* in Ras^{V12}-expressing tissues could influence their ability to outcompete wild-type cells or cause a cell cycle delay that promotes cell differentiation, as it has been previously shown that *prp8* regulates G2/M transition (Andersen and Tapon, 2008).

Interestingly, we also observed a role for *prp8* in the regulation of Ras^{V12}-induced hyperplasia in the adult gut. Depletion of *prp8* in Ras^{V12}-expressing tissues significantly reduced hyperplasia and the cells no longer invade the gut lumen. Despite this, we failed to detect increased levels of apoptosis in Ras^{V12}; $prp8^{RNAi}$ cells compared with cells expressing Ras^{V12} alone, which is consistent with our observations in the eye disc. However, we did not detect cell differentiation changes in the adult gut, at least at the level of the ee population. Our results do not rule out an effect of *prp8* in the regulation of EC differentiation, which could potentially be masked by the fact that the majority of the cell renewal in the gut involves ECs (Guo et al., 2016). However, we would favour the hypothesis that Prp8 affects mostly proliferation or stem cell dynamics, rather than directly affecting differentiation, as the number of GFP-positive cells and ISCs was reduced when *prp8* was depleted. Our data indicate that the precise mechanism by which *prp8* regulates oncogene-induced hyperplasia may differ according to the affected tissue. Consistent with this, despite presumably regulating splicing ubiquitously, mutations in the human orthologue of *prp8*, *PRPF8*, are generally only associated with diseases in specific organs, such as retinitis pigmentosa which affects the eye (Grainger and Beggs, 2005).

Our results also raise issues regarding the role of the spliceosome in the regulation of tumour growth. We found that depletion of spliceosome components resulted in suppression of Ras^{V12}-induced hyperplasia. This would suggest that *prp8* regulates Ras^{V12}-mediated hyperplasia through its function within the spliceosome. This would be in agreement with the observation that mutation in other spliceosome components besides *PRPF8* can cause retinitis pigmentosa in humans (Krausova and Stanek, 2017). However, in the context of oncogenic RET, we found that *prp8* depletion enhances the RET phenotype, whereas depleting other spliceosome components suppresses it. This would suggest that Prp8 regulates RET^{MEN2B}-mediated hyperplasia and invasion in a spliceosome-independent manner, which requires further investigation. Notably, it has been previously shown that other spliceosome components have pleiotropic roles and additional non-splicing-related functions, as exemplified by Prp19 (Chanarat and Strasser, 2013). It will also be important to determine the molecular requirements for the function of *prp8* in the regulation of hyperplasia, that is, which are the protein domains involved. Prp8 is considered to be an inactive DUB because of specific amino acid alterations in the MPN/JAB domain that serves as the catalytic domain in JAMM family DUBs (Clague et al., 2013; Grainger and Beggs, 2005; Komander et al., 2009; Pena et al., 2007). However, as the Prp8 MPN/JAB domain is essential for its function and can bind ubiquitin, it is possible that the role of Prp8 requires this domain and that it may involve the interaction of Prp8 with ubiquitylated proteins (Bellare et al., 2006). Detailed *in vivo* structure-function analysis will be required to fully elucidate this point but, interestingly, previous studies have suggested that ubiquitylation is important for the modulation of spliceosome protein-protein interactions (Das et al., 2017; Song et al., 2010). As for the downstream mechanisms involved, our data do not support a major role for modulation of the MAPK signalling cascade. Despite the fact that previous studies have shown that alterations in spliceosome genes cause dramatic changes in the splicing pattern of MAPK and affect Ras downstream signalling, we failed to uncover a major effect of Prp8 in this process and, accordingly, expressing MAPK in $prp8^{RNAi}$ tissues was insufficient to rescue their hypoplasia (Ashton-Beaucage et al., 2014).

Prp8 appears to be required for Ras-driven hyperplasia and this role appears to be conserved with other oncogenes, such as activated *Egfr* and *N*. Therefore, our data extends recent observations in the context of human cancers, in which the spliceosome has been identified as a potential therapeutic target in Myc-driven tumours (Hsu et al., 2015). Our results suggest that Prp8 could be a specific target in tumours driven not only by Ras, Notch and EGFR but, potentially, by other receptor tyrosine kinases that signal through Ras and downstream pathways. However, as *prp8* depletion enhanced the phenotype of RET^{MEN2B} in the developing wing, it will be important to define the mechanisms that control the function of Prp8 (and of the spliceosome) in the regulation of hyperplasia and tumour growth. In conclusion, clearly more work is needed to determine in which conditions inhibiting the spliceosome will be beneficial for cancer treatment.

MATERIALS AND METHODS

Fly strains and genetic crosses

MARCM experiments were performed using the *y, w, hsFLP, UAS-GFP-nls; tub-Gal4, FRT42D tub-Gal80* MARCM maker stock. Below are the respective genotypes for the MARCM experiment: *y, w, hsFLP, UAS-GFP-nls; tub-Gal4, FRT42D tub-Gal80/FRT42D blank* (Fig. 1J); *y, w, hsFLP, UAS-GFP-nls; tub-Gal4, FRT42D tub-Gal80/FRT42D blank; +/UAS-*Ras^{V12} (Fig. 1K); *y, w, hsFLP, UAS-GFP-nls; tub-Gal4, FRT42D tub-Gal80/FRT42D* $prp8^{KG03188}$ (Fig. 1L); and *y, w, hsFLP, UAS-GFP-*

Development (2018) 145, dev162156. doi:10.1242/dev.162156

nls; tub-Gal4, FRT42D tub-Gal80/FRT42D prp8^{KG03188}*; +/UAS-Ras*^{V12} (Fig. 1M).

For additional details of fly strains used, see supplementary Materials and Methods.

Immunostaining

Third instar larval imaginal discs and adult guts were dissected in PBS and fixed for 20-30 min at room temperature (RT) in PBS containing 4% formaldehyde. After washing with 0.1% Triton X-100 (TX)/PBS, tissues were permeabilised with 0.1% or 0.3% TX/PBS for 30 min and, following additional washing steps with 0.1% TX/PBS (five times for 5 min), blocked for 30 min in blocking buffer [10% normal goat serum (NGS), 0.1% TX/PBS] and incubated overnight at 4°C with primary antibody diluted in blocking buffer. After washing with 0.1% TX/PBS and a blocking step, tissues were incubated for 1-4 h at RT with secondary antibodies. Samples were mounted in Vectashield (Vector Laboratories) after additional washing steps. For F-actin and DNA staining, tissues were incubated with TRITC-conjugated phalloidin (1:500; Sigma-Aldrich) or Hoechst 33342 (1:1000; Thermo Fisher Scientific), respectively, for 15 min during one of the final washing steps.

Antibodies

The following antibodies were used: rabbit anti-GFP (A-11122; Thermo Fisher Scientific; 1:1000), mouse anti-GFP (A-11120; Thermo Fisher Scientific; 1:1000) or chicken anti-GFP (ab13970; Abcam; 1:1000); rabbit anti-cleaved Caspase 3 (DCP-1) (9578; Cell Signaling Technology, 1:250); rabbit anti-phospho Histone H3 Ser10 (06-570; Merck; 1:1000); mouse anti-Dlg [4F3; Developmental Studies Hybridoma Bank (DSHB); 1:250]; rat anti-Elav (7E8A10; DSHB; 1:10); mouse anti-Repo (8D12; DSHB; 1:10); mouse anti-Delta (C594.9B; DSHB; 1:100); mouse anti-Prospero (MR1A; DSHB; 1:20); mouse anti-BrdU (G3G4; DSHB; 1:10); mouse anti-Cyclin B (F2F4; DSHB; 1:5); mouse anti-Eya (eya10H6; DSHB; 1:100); rabbit anti-MAPK (M5670; Sigma-Aldrich; 1:500) rabbit anti-phospho-MAPK (p44/42 MAPK ERK1/2–137F5; Cell Signaling Technology; 1:500). Secondary antibodies used were coupled to FITC (1:1000), Alexa Fluor 488, Alexa Fluor 568, Alexa Fluor 633, Alexa Fluor 647 (1:2000), Cy3 or Cy5 (1:200 or 1:500, depending on the primary antibody used) (Molecular Probes).

BrdU analysis

BrdU analysis was performed as previously reported (Chioda et al., 2010). Briefly, wandering third instar larvae were collected and eye imaginal discs were dissected in PBS. Discs were incubated in 1× PBS containing 20 µM BrdU (Sigma-Aldrich) for 30 min. Discs were fixed in PBS with 4% formaldehyde for 30 min at RT. DNA was denatured with 3 M HCl for 30 min. Samples were washed 3× with PBS containing 0.3% TX, followed by incubation in blocking buffer (10% NGS, 0.1% TX/PBS) for 1 h. Samples were incubated with mouse anti-BrdU antibody (G3G4; DSHB; 1:10) overnight at 4°C. Subsequent steps were performed as described in the immunostaining section.

Analysis of cell numbers in adult gut

Nuclei were segmented in 3D using a user-defined fluorescence threshold and watershed to separate nuclei in contact. Segmented nuclei were then classified into big or small cells based on their volume (the threshold was ∼90 µm^3 but it was optimised for each image) and within each category they were classified as part of a clone or not based on their mean green intensity value, which was also optimised for each image. To avoid changes in fluorescence owing to the depth of the tissue, only nuclei in the half of the gut closest to the coverslip were considered. The code was implemented in Matlab and is available at github.com/juliafs93/CellCounter.

Drosophila cell culture and expression constructs

Drosophila S2 cells were grown in *Drosophila* Schneider's medium (Thermo Fisher Scientific) supplemented with 10% (v/v) foetal bovine serum, 50 µg/ml penicillin and 50 µg/ml streptomycin. Expression plasmids were transfected using Effectene transfection reagent (Qiagen) according to the manufacturer's instructions. Expression plasmids were generated using Gateway technology (Thermo Fisher Scientific). All vectors were verified by sequencing. S2 cells and the Ras^{V12} cDNA were a kind gift from Nic Tapon (The Francis Crick Institute, London, UK).

dsRNA production and treatment

dsRNAs were synthesised using the Megascript T7 kit (Thermo Fisher Scientific) according to the manufacturer's instructions. DNA templates for dsRNA synthesis were PCR amplified from genomic DNA or from plasmids that encoded the respective genes using primers that contained the 5′ T7 RNA polymerase-binding site sequence. dsRNA primers were designed using the DKFZ RNAi design tool (www.dkfz.de/signaling/e-rnai3). The following primers were used: *lacZ* (forward, TTGCCGGGAAGCTAGAGTAA; reverse, GCCTTCCTGTTTTTGCTCAC) and *prp8* (forward, CGAGTCTGGCTGTTCTTTATGC; reverse, ATGTACGGACCGTCCTTTAAGTAG). After seeding, S2 cells were incubated with 15-20 µg dsRNA for 1 h in serum-free medium, before complete medium was added. Cells were lysed and processed for further analysis 72 h after dsRNA treatment.

RNA isolation and RT-PCR analysis

Total RNAi was extracted from S2 cells using the QIAshredder and RNeasy kits (Qiagen) according to the manufacturer's protocols. RNA purity and concentration were assessed using a Nanodrop One UV-Vis spectrophotometer (Thermo Fisher Scientific). cDNA was synthesised using the QuantiTect Reverse Transcription kit (Qiagen) following the manufacturer's instructions. RT-PCR analysis was performed using 1 µl of cDNA per PCR reaction and the following primers: MAPK full-length (forward, CGCCGTCGATTTTGATAAATCATATTTACGC; reverse, AGGCGCATTGTCTGGTTGTCGT) (Ashton-Beaucage et al., 2014). RT-PCR products were run in 2% UltraPure agarose (Thermo Fisher Scientific) gels and imaged in an Amersham Imager 600 (GE Healthcare).

Image acquisition and analysis

For *in vivo* RNAi screen studies, whole larva images were acquired using a Zeiss SteREO Lumar V12 stereomicroscope. Confocal images were acquired at ×20 or ×40 magnification using a Zeiss LSM710 confocal microscope or an Olympus FV1000 confocal microscope equipped with 20×/0.85 oil and 40×/1.35 oil iris objectives. All images were taken as *z*-stacks of 1 µm sections in eye and wing imaginal discs and in the posterior midgut region immediately anterior to the hindgut (R4-R5 region). For cross-sections and 3D reconstructions, images were acquired as *z*-stacks of optimal sections. Image processing, analysis and 3D reconstruction were performed with ImageJ and Imaris XT8.0.

Quantification and statistical analyses

3D reconstruction images were quantified using Imaris 8.4 and ImageJ and quantifications were performed throughout the volume of the reconstruction. GFP area was calculated in 3D volume using Imaris 8.4 or ImageJ. Quantification of cell numbers, Delta-positive and Prospero-positive cells was performed manually in ImageJ. Statistical analyses were performed in Microsoft Excel or GraphPad Prism. Significance (*P*) values were determined using one-way ANOVA analysis (with Tukey's post test for multiple comparisons or Kruskal–Wallis and Dunn post tests for non-parametric *t*-tests). Unless otherwise stated, data is represented as mean±s.e.m.

Acknowledgements

We thank the Transgenic RNAi Project (TRiP) at Harvard Medical School [National Institutes of Health (NIH)/National Institute of General Medical Sciences, R01-GM084947], the Kyoto Stock Center (DGRC) and the Vienna *Drosophila* Resource Center for providing transgenic RNAi fly stocks used in this study. Stocks obtained from the Bloomington *Drosophila* Stock Center (NIH P40OD018537) were used in this study. We thank Ross Cagan, Sarah Bray, Nic Tapon, Barry Thompson and Pascal Meier for fly stocks. We thank Pascal Meier for compiling the first iteration of the *Drosophila in vivo* DUB RNAi library and for assistance in assembling the current library. The antibodies 4F3, 8D12, 7E8A10, C594.9B, MR1A, G3G4, F2F4 and eya10H6, developed by C. Goodman (4F3 and 8D12), G. Rubin, S. Artavanis-Tsakonas, C. Doe, S. J. Kaufman, P. H. O'Farrell, and S. Benzer and N. M. Bonini (eya10H6), were obtained from the Developmental Studies Hybridoma Bank, which was created by the National Institute of Child Health and Human Development of the

NIH and maintained at The University of Iowa, Department of Biology. We thank Linda Hammond for assistance with microscopy. We thank Nick Brown for support and access to microscopy facilities. We thank members of the Ribeiro lab for helpful discussions and comments on the manuscript. We thank Sarah Martin, Susana Godinho, Tyson Sharp, Prabhakar Rajan, Pascal Meier and Nic Tapon for critical reading of the manuscript.

Competing interests

The authors declare no competing or financial interests.

Author contributions

Conceptualization: C.H.F.-E., P.S.R.; Methodology: C.H.F.-E., A.R., A.D.F., J.F.-S., P.S.R.; Software: J.F.-S.; Validation: C.H.F.-E., A.R., P.S.R.; Formal analysis: C.H.F.-E., A.R., A.D.F., J.F.-S., P.S.R.; Investigation: C.H.F.-E., A.R., A.D.F., D.G.-G., P.S.R.; Resources: C.H.F.-E., A.D.F., J.F.-S., P.S.R.; Writing - original draft: C.H.F.-E., P.S.R.; Writing - review & editing: C.H.F.-E., A.R., A.D.F., P.S.R.; Visualization: C.H.F.-E., P.S.R.; Supervision: P.S.R.; Project administration: P.S.R.; Funding acquisition: P.S.R.

Funding

This work was supported by funding from Cancer Research UK (C16420/A18066), The Brain Tumour Charity (GN-000408) and The Academy of Medical Sciences/ Wellcome Trust Springboard Award (SBF001/1018). Deposited in PMC for immediate release.

Supplementary information

Supplementary information available online at
http://dev.biologists.org/lookup/doi/10.1242/dev.162156.supplemental

References

Amcheslavsky, A., Jiang, J. and Ip, Y. T. (2009). Tissue damage-induced intestinal stem cell division in Drosophila. *Cell Stem Cell* **4**, 49-61.

Andersen, D. S. and Tapon, N. (2008). Drosophila MFAP1 is required for pre-mRNA processing and G2/M progression. *J. Biol. Chem.* **283**, 31256-31267.

Ashton-Beaucage, D., Udell, C. M., Gendron, P., Sahmi, M., Lefrançois, M., Baril, C., Guenier, A.-S., Duchaine, J., Lamarre, D., Lemieux, S. et al. (2014). A functional screen reveals an extensive layer of transcriptional and splicing control underlying RAS/MAPK signaling in Drosophila. *PLoS Biol.* **12**, e1001809.

Bellare, P., Kutach, A. K., Rines, A. K., Guthrie, C. and Sontheimer, E. J. (2006). Ubiquitin binding by a variant Jab1/MPN domain in the essential pre-mRNA splicing factor Prp8p. *RNA* **12**, 292-302.

Bieging, K. T., Mello, S. S. and Attardi, L. D. (2014). Unravelling mechanisms of p53-mediated tumour suppression. *Nat. Rev. Cancer* **14**, 359-370.

Bonini, N. M., Leiserson, W. M. and Benzer, S. (1993). The eyes absent gene: genetic control of cell survival and differentiation in the developing Drosophila eye. *Cell* **72**, 379-395.

Broemer, M., Tenev, T., Rigbolt, K. T. G., Hempel, S., Blagoev, B., Silke, J., Ditzel, M. and Meier, P. (2010). Systematic in vivo RNAi analysis identifies IAPs as NEDD8-E3 ligases. *Mol. Cell* **40**, 810-822.

Brumby, A. M., Goulding, K. R., Schlosser, T., Loi, S., Galea, R., Khoo, P., Bolden, J. E., Aigaki, T., Humbert, P. O. and Richardson, H. E. (2011). Identification of novel Ras-cooperating oncogenes in Drosophila melanogaster: a RhoGEF/Rho-family/JNK pathway is a central driver of tumorigenesis. *Genetics* **188**, 105-125.

Cagan, R. (2009). Principles of Drosophila eye differentiation. *Curr. Top. Dev. Biol.* **89**, 115-135.

Chabu, C., Li, D.-M. and Xu, T. (2017). EGFR/ARF6 regulation of Hh signalling stimulates oncogenic Ras tumour overgrowth. *Nat. Commun.* **8**, 14688.

Chanarat, S. and Strasser, K. (2013). Splicing and beyond: the many faces of the Prp19 complex. *Biochim. Biophys. Acta* **1833**, 2126-2134.

Chioda, M., Vengadasalam, S., Kremmer, E., Eberharter, A. and Becker, P. B. (2010). Developmental role for ACF1-containing nucleosome remodellers in chromatin organisation. *Development* **137**, 3513-3522.

Clague, M. J., Barsukov, I., Coulson, J. M., Liu, H., Rigden, D. J. and Urbé, S. (2013). Deubiquitylases from genes to organism. *Physiol. Rev.* **93**, 1289-1315.

Claudius, A.-K., Romani, P., Lamkemeyer, T., Jindra, M. and Uhlirova, M. (2014). Unexpected role of the steroid-deficiency protein ecdysoneless in pre-mRNA splicing. *PLoS Genet.* **10**, e1004287.

Coelho, C. M. A., Kolevski, B., Walker, C. D., Lavagi, I., Shaw, T., Ebert, A., Leevers, S. J. and Marygold, S. J. (2005). A genetic screen for dominant modifiers of a small-wing phenotype in Drosophila melanogaster identifies proteins involved in splicing and translation. *Genetics* **171**, 597-614.

Das, T. K., Sangodkar, J., Negre, N., Narla, G. and Cagan, R. L. (2013). Sin3a acts through a multi-gene module to regulate invasion in Drosophila and human tumors. *Oncogene* **32**, 3184-3197.

Das, T., Park, J. K., Park, J., Kim, E., Rape, M., Kim, E. E. and Song, E. J. (2017). USP15 regulates dynamic protein-protein interactions of the spliceosome through deubiquitination of PRP31. *Nucleic Acids Res.* **45**, 4866-4880.

Fic, W., Juge, F., Soret, J. and Tazi, J. (2007). Eye development under the control of SRp55/B52-mediated alternative splicing of eyeless. *PLoS ONE* **2**, e253.

Fraile, J. M., Quesada, V., Rodríguez, D., Freije, J. M. P. and López-Otín, C. (2012). Deubiquitinases in cancer: new functions and therapeutic options. *Oncogene* **31**, 2373-2388.

Gonzalez, C. (2013). Drosophila melanogaster: a model and a tool to investigate malignancy and identify new therapeutics. *Nat. Rev. Cancer* **13**, 172-183.

Grainger, R. J. and Beggs, J. D. (2005). Prp8 protein: at the heart of the spliceosome. *RNA* **11**, 533-557.

Guinea-Viniegra, J., Zenz, R., Scheuch, H., Jiménez, M., Bakiri, L., Petzelbauer, P. and Wagner, E. F. (2012). Differentiation-induced skin cancer suppression by Fos, p53, and TACE/ADAM17. *J. Clin. Invest.* **122**, 2898-2910.

Guo, Z., Lucchetta, E., Rafel, N. and Ohlstein, B. (2016). Maintenance of the adult Drosophila intestine: all roads lead to homeostasis. *Curr. Opin. Genet. Dev.* **40**, 81-86.

Hanahan, D. and Weinberg, R. A. (2011). Hallmarks of cancer: the next generation. *Cell* **144**, 646-674.

Heride, C., Urbé, S. and Clague, M. J. (2014). Ubiquitin code assembly and disassembly. *Curr. Biol.* **24**, R215-R220.

Hsu, T. Y.-T., Simon, L. M., Neill, N. J., Marcotte, R., Sayad, A., Bland, C. S., Echeverria, G. V., Sun, T., Kurley, S. J., Tyagi, S. et al. (2015). The spliceosome is a therapeutic vulnerability in MYC-driven cancer. *Nature* **525**, 384-388.

Hynes, N. E., Ingham, P. W., Lim, W. A., Marshall, C. J., Massagué, J. and Pawson, T. (2013). Signalling change: signal transduction through the decades. *Nat. Rev. Mol. Cell Biol.* **14**, 393-398.

Jiang, H., Patel, P. H., Kohlmaier, A., Grenley, M. O., Mcewen, D. G. and Edgar, B. A. (2009). Cytokine/Jak/Stat signaling mediates regeneration and homeostasis in the Drosophila midgut. *Cell* **137**, 1343-1355.

Jiang, H., Grenley, M. O., Bravo, M.-J., Blumhagen, R. Z. and Edgar, B. A. (2011). EGFR/Ras/MAPK signaling mediates adult midgut epithelial homeostasis and regeneration in Drosophila. *Cell Stem Cell* **8**, 84-95.

Keightley, M.-C., Crowhurst, M. O., Layton, J. E., Beilharz, T., Markmiller, S., Varma, S., Hogan, B. M., de Jong-Curtain, T. A., Heath, J. K. and Lieschke, G. J. (2013). In vivo mutation of pre-mRNA processing factor 8 (Prpf8) affects transcript splicing, cell survival and myeloid differentiation. *FEBS Lett.* **587**, 2150-2157.

Komander, D., Clague, M. J. and Urbé, S. (2009). Breaking the chains: structure and function of the deubiquitinases. *Nat. Rev. Mol. Cell Biol.* **10**, 550-563.

Krausova, M. and Stanek, D. (2017). snRNP proteins in health and disease. *Semin. Cell Dev. Biol.* **79**, 92-102.

Lee, B. P. and Jones, B. W. (2005). Transcriptional regulation of the Drosophila glial gene repo. *Mech. Dev.* **122**, 849-862.

Lee, T., Feig, L. and Montell, D. J. (1996). Two distinct roles for Ras in a developmentally regulated cell migration. *Development* **122**, 409-418.

Micchelli, C. A. and Perrimon, N. (2006). Evidence that stem cells reside in the adult Drosophila midgut epithelium. *Nature* **439**, 475-479.

Ohlstein, B. and Spradling, A. (2006). The adult Drosophila posterior midgut is maintained by pluripotent stem cells. *Nature* **439**, 470-474.

Ohsawa, S., Sato, Y., Enomoto, M., Nakamura, M., Betsumiya, A. and Igaki, T. (2012). Mitochondrial defect drives non-autonomous tumour progression through Hippo signalling in Drosophila. *Nature* **490**, 547-551.

Pagliarini, R. A. and Xu, T. (2003). A genetic screen in Drosophila for metastatic behavior. *Science* **302**, 1227-1231.

Pallavi, S. K., Ho, D. M., Hicks, C., Miele, L. and Artavanis-Tsakonas, S. (2012). Notch and Mef2 synergize to promote proliferation and metastasis through JNK signal activation in Drosophila. *EMBO J.* **31**, 2895-2907.

Pastor-Pareja, J. C. and Xu, T. (2013). Dissecting social cell biology and tumors using Drosophila genetics. *Annu. Rev. Genet.* **47**, 51-74.

Pena, V., Liu, S., Bujnicki, J. M., Lührmann, R. and Wahl, M. C. (2007). Structure of a multipartite protein-protein interaction domain in splicing factor prp8 and its link to retinitis pigmentosa. *Mol. Cell* **25**, 615-624.

Pickup, A. T., Lamka, M. L., Sun, Q., Yip, M. L. and Lipshitz, H. D. (2002). Control of photoreceptor cell morphology, planar polarity and epithelial integrity during Drosophila eye development. *Development* **129**, 2247-2258.

Queenan, A. M., Ghabrial, A. and Schupbach, T. (1997). Ectopic activation of torpedo/Egfr, a Drosophila receptor tyrosine kinase, dorsalizes both the eggshell and the embryo. *Development* **124**, 3871-3880.

Ragab, A., Buechling, T., Gesellchen, V., Spirohn, K., Boettcher, A.-L. and Boutros, M. (2011). Drosophila Ras/MAPK signalling regulates innate immune responses in immune and intestinal stem cells. *EMBO J.* **30**, 1123-1136.

Rape, M. (2017). Ubiquitylation at the crossroads of development and disease. *Nat. Rev. Mol. Cell Biol.* **19**, 59-70.

Read, R. D., Goodfellow, P. J., Mardis, E. R., Novak, N., Armstrong, J. R. and Cagan, R. L. (2005). A Drosophila model of multiple endocrine neoplasia type 2. *Genetics* **171**, 1057-1081.

Restivo, G., Nguyen, B.-C., Dziunycz, P., Ristorcelli, E., Ryan, R. J. H., Özuysal, O. Y., DI Piazza, M., Radtke, F., Dixon, M. J., Hofbauer, G. F. L. et al. (2011).

IRF6 is a mediator of Notch pro-differentiation and tumour suppressive function in keratinocytes. *EMBO J.* **30**, 4571-4585.
Roignant, J.-Y. and Treisman, J. E. (2010). Exon junction complex subunits are required to splice Drosophila MAP kinase, a large heterochromatic gene. *Cell* **143**, 238-250.
Rudrapatna, V. A., Cagan, R. L. and Das, T. K. (2012). Drosophila cancer models. *Dev. Dyn.* **241**, 107-118.
Rudrapatna, V. A., Bangi, E. and Cagan, R. L. (2013). Caspase signalling in the absence of apoptosis drives Jnk-dependent invasion. *EMBO Rep.* **14**, 172-177.
Rusconi, J. C., Hays, R. and Cagan, R. L. (2000). Programmed cell death and patterning in Drosophila. *Cell Death Differ.* **7**, 1063-1070.
Shi, Y. (2017). The spliceosome: a protein-directed metalloribozyme. *J. Mol. Biol.* **429**, 2640-2653.
Silies, M., Yuva-Aydemir, Y., Franzdottir, S. R. and Klämbt, C. (2010). The eye imaginal disc as a model to study the coordination of neuronal and glial development. *Fly (Austin)* **4**, 71-79.
Soller, M. and White, K. (2004). Elav. *Curr. Biol.* **14**, R53.
Song, E. J., Werner, S. L., Neubauer, J., Stegmeier, F., Aspden, J., Rio, D., Harper, J. W., Elledge, S. J., Kirschner, M. W. and Rape, M. (2010). The Prp19 complex and the Usp4Sart3 deubiquitinating enzyme control reversible ubiquitination at the spliceosome. *Genes Dev.* **24**, 1434-1447.
Sonoshita, M. and Cagan, R. L. (2017). Modeling human cancers in Drosophila. *Curr. Top. Dev. Biol.* **121**, 287-309.
Tipping, M. and Perrimon, N. (2014). Drosophila as a model for context-dependent tumorigenesis. *J. Cell. Physiol.* **229**, 27-33.
Wu, H., Sun, L., Wen, Y., Liu, Y., Yu, J., Mao, F., Wang, Y., Tong, C., Guo, X., Hu, Z. et al. (2016). Major spliceosome defects cause male infertility and are associated with nonobstructive azoospermia in humans. *Proc. Natl. Acad. Sci. USA* **113**, 4134-4139.
Zeng, X., Singh, S. R., Hou, D. and Hou, S. X. (2010). Tumor suppressors Sav/Scrib and oncogene Ras regulate stem-cell transformation in adult Drosophila malpighian tubules. *J. Cell. Physiol.* **224**, 766-774.

Supplementary Materials and Methods

Fly stocks

The *UAS-DUB^{RNAi}* library (Supplementary Table 1) was compiled in collaboration with Pascal Meier (Institute of Cancer Research, UK). *UAS-Ras^{V12}* **(Lee et al., 1996)**, *UAS-EGFR$^{\lambda Top4.1}$* **(Queenan et al., 1997)**, *UAS-DIAP1*, *UAS-p35* and the Ras^{V12} cDNA were kind gifts from Nic Tapon. *UAS-RET^{MEN2B}* **(Read et al., 2005)** was a kind gift from Ross Cagan. *UAS-N$^{\Delta ECD}$* was a kind gift from Sarah Bray. The FRT42D MARCM maker stock was a kind gift from Barry Thompson. The *prp8^{KG03188}* allele was obtained from the Kyoto Stock Center (DGRC). Other stocks were obtained from the Bloomington Stock Centre. More information regarding *Drosophila* genes and stocks is available on FlyBase (http://flybase.org).

Fly genotypes

Fig. 1A, 1E, 2A, 2E, 3A, 3E, 3I, 4A, 4E, S2A, S3A, S3E, S3M: *eyFLP; tub-Gal80^{ts}; act<CD2<Gal4, UAS-GFP*

Fig. 1B, 1F, 2B, 2F, 3B, 3F, 3J, 4B, 4F, S1D, S2B, S3B, S3F: *eyFLP/+; tub-Gal80^{ts}/UAS-Ras^{V12}; act<CD2<Gal4, UAS-GFP/TM6B*

Fig. 1C, 1G, 2C, 2G, 3C, 3G, 3K, 4C, 4G, S2C, S3C, S3G, S3N: *eyFLP/+; tub-Gal80^{ts}/+; act<CD2<Gal4, UAS-GFP/ UAS-prp8^{RNAi} (18567GD)*

Fig. 1D, 1H, 2D, 2H, 3D, 3H, 3L, 4D, 4H, S2D, S3D, S3H: *eyFLP/+; tub-Gal80^{ts}/UAS-Ras^{V12}; act4<CD2<Gal4, UAS-GFP/UAS-prp8^{RNAi} (18567GD)*

Fig. 1J: *y, w, hsFLP, UAS-GFP-nls; tub-Gal4, FRT42D tub-Gal80/FRT42D blank*

Fig. 1K: *y, w, hsFLP, UAS-GFP-nls; tub-Gal4, FRT42D tub-Gal80/FRT42D blank; +/UAS-Ras^{V12}*

Fig. 1L: *y, w, hsFLP, UAS-GFP-nls; tub-Gal4, FRT42D tub-Gal80/FRT42D prp8^{KG03188}*

Fig. 1M: *y, w, hsFLP, UAS-GFP-nls; tub-Gal4, FRT42D tub-Gal80/FRT42D prp8^{KG03188}; +/UAS-Ras^{V12}*

Fig. 5B, 6A, S5A, S5E, S6A: *yw; esg-Gal4; tub-Gal80^{ts}, UAS-GFP*

Fig. 5C, 6B, S5B, S5F, S6B: *yw; esg-Gal4/UAS-Ras^{V12}; tub-Gal80^{ts}, UAS-GFP/+*

Fig. 5D, 6C, S5C, S5G, S6C: *yw; esg-Gal4/+; tub-Gal80^{ts}, UAS-GFP/ UAS-prp8^{RNAi} (18567GD)*

Fig. 5E, 6D, S5D, S5H, S6D: *yw; esg-Gal4/ UAS-Ras^{V12}; tubGal80^{ts}, UAS-GFP/ UAS-prp8^{RNAi} (18567GD)*

Fig. 6E: *yw; esg-Gal4/UAS-P35; tub-Gal80^{ts}, UAS-GFP/+*

Fig. 6F: *yw; esg-Gal4/UAS-P35; tub-Gal80^{ts}, UAS-GFP/ UAS-prp8^{RNAi} (18567GD)*

Fig. 7A, S7A: *w; ptc-Gal4, UAS-CD8-GFP/+*

Fig. 7B, S7B: *w; ptc-Gal4, UAS-CD8-GFP/+; UAS-RET$^{MEN2B\ (M955T)}$/+*

Fig. 7C, S7C: *w; ptc-Gal4, UAS-CD8-GFP/UAS-prp8^{RNAi} (18565GD)*

Fig. 7D, S7D: *w; ptc-Gal4, UAS-CD8-GFP/ UAS-prp8^{RNAi} (18565GD); UAS-RET$^{MEN2B\ (M955T)}$/+*

Fig. S1B: *eyFLP/+; tub-Gal80^{ts}/UAS-Usp10^{RNAi} (37858GD); act<CD2<Gal4, UAS-GFP/+*

Fig. S1C: *eyFLP/+; tub-Gal80^{ts}/UAS-Npl4^{RNAi} (4673R-2); act<CD2<Gal4, UAS-GFP/+*

Fig. S1E: *eyFLP/+; tub-Gal80^{ts}/UAS-lgl^{RNAi}; act<CD2<Gal4, UAS-GFP/UAS-Ras^{V12}*

Fig. S1F: *eyFLP/+; tub-Gal80^{ts}/UAS-Ras^{V12}; act<CD2<Gal4, UAS-GFP/UAS-scrib^{RNAi}*

Fig. S1G: *eyFLP/+; tub-Gal80^{ts}/UAS-baz^{RNAi}; act<CD2<Gal4, UAS-GFP/UAS-Ras^{V12}*

Fig. S1H: *eyFLP/+; tub-Gal80^{ts}/UAS-Usp10^{RNAi} (37858GD); act<CD2<Gal4, UAS-GFP/UAS-Ras^{V12}*

Fig. S1I: *eyFLP/+; tub-Gal80^{ts}/UAS-Npl4^{RNAi} (4673R-2); act<CD2<Gal4, UAS-GFP/UAS-Ras^{V12}*

Fig. S1J: *eyFLP/+; tub-Gal80^{ts}/UAS- Ras^{V12}; act<CD2<Gal4, UAS-GFP/UAS-Usp47^{RNAi}*

Fig. S1K: *eyFLP/+; tub-Gal80^{ts}/UAS-not^{RNAi} (45776GD); act<CD2<Gal4, UAS-GFP/UAS-Ras^{V12}*

Fig. S2F: *eyFLP/+; tub-Gal80^{ts}/UAS-P35; act<CD2<Gal4, UAS-GFP/+*

Fig. S2G: *eyFLP/+; tub-Gal80^{ts}/UAS-P35; act<CD2<Gal4, UAS-GFP/UAS-prp8^{RNAi} (18567GD)*

Fig. S3O: *eyFLP/+; tub-Gal80^{ts}/UAS-rl; act<CD2<Gal4, UAS-GFP/UAS-prp8^{RNAi} (18567GD)*

Fig. S4A: *eyFLP/UAS-EGFR$^{\lambda Top4.1}$; tub-Gal80^{ts}/+; act<CD2<Gal4, UAS-GFP/+*

Fig. S4B: *eyFLP/UAS-EGFR$^{\lambda Top4.1}$; tub-Gal80^{ts}/+; act<CD2<Gal4, UAS-GFP/UAS-prp8^{RNAi} (18567GD)*

Fig. S4C: *eyFLP/+; tub-Gal80^{ts}/UAS-N^{ECD}; act<CD2<Gal4, UAS-GFP/MKRS*

Fig. S4D: *eyFLP/+; tub-Gal80^{ts}/UAS-N^{ECD}; act<CD2<Gal4, UAS-GFP/UAS-prp8^{RNAi} (18567GD)*

Fig. S4E: *eyFLP/+; tub-Gal80^{ts}/UAS-mfap1^{RNAi} (103419KK); act<CD2<Gal4, UAS-GFP/+*

Fig. S4F: *eyFLP/+; tub-Gal80^{ts}/UAS-mfap1^{RNAi} (103419KK); act<CD2<Gal4, UAS-GFP/UAS-Ras^{V12}*

Fig. S4G: *eyFLP/+; tub-Gal80^{ts}/UAS-prp38^{RNAi} (110282KK); act<CD2<Gal4, UAS-GFP/+*

Fig. S4H: *eyFLP/+; tub-Gal80^{ts}/UAS-prp38^{RNAi} (110282KK); act<CD2<Gal4, UAS-GFP/UAS-Ras^{V12}*

Fig. S4I: *eyFLP/+; tub-Gal80^{ts}/+; act4<CD2<Gal4, UAS-GFP/UAS-bx42^{RNAi} (34777 TRiP)*

Fig. S4J: *eyFLP/+; tub-Gal80^{ts}/UAS-Ras^{V12}; act4<CD2<Gal4, UAS-GFP/UAS-bx42^{RNAi} (34777 TRiP)*

Fig. S7E: *w*; *ptc-Gal4, UAS-CD8-GFP/UAS-mfap1^{RNAi} (103419KK)*

Fig. S7F: *w*; *ptc-Gal4, UAS-CD8-GFP/UAS-mfap1^{RNAi} (103419KK); UAS-RET$^{MEN2B\ (M955T)}$/+*

Fig. S7G: *w; ptc-Gal4, UAS-CD8-GFP/UAS-prp38^{RNAi} (110282KK)*

Fig. S7H: *w; ptc-Gal4, UAS-CD8-GFP/ UAS-prp38^{RNAi} (110282KK); UAS-RET$^{MEN2B\ (M955T)}$/+*

Fig. S7I: *w*; *ptc-Gal4, UAS-CD8-GFP/+; UAS-bx42^{RNAi} (34777 TRiP)/+*

Fig. S7J: *w*; *ptc-Gal4, UAS-CD8-GFP/+; UAS-bx42^{RNAi} (34777 TRiP)/UAS-RET$^{MEN2B\ (M955T)}$*

Wing imaginal disc experiments were performed with *ptc-Gal4, UAS-CD8-GFP* (Nic Tapon). Crosses were performed at 25ºC until wandering L3 larvae were observed, collected and dissected.

Eye imaginal disc experiments were performed with *eyFLP*; *tub-Gal80^{ts}*; *act<CD2<Gal4*, *UAS-GFP*. Crosses were maintained at 18ºC for 120h before switching to 29ºC for induction of gene expression. Similar to wing imaginal disc experiments, wandering L3 larvae were collected and dissected after approximately 2-3 days at 29ºC.

Adult gut experiments were performed with *esg-Gal4*; *UAS-GFP*, *tub-Gal80^{ts}*. Crosses were maintained at 18ºC and flipped every 48 hours. Newly eclosed adult flies were collected and kept for 2 days at 18ºC before shifting to 29ºC for 2-7 days before dissection. Unless otherwise specified, all adult gut analyses were performed 7 days after transgene expression.

Mosaic analysis with a repressible cell marker (MARCM) clone experiments were performed with *y,w, hsFLP, UAS-GFP-nls; tub-Gal4, FRT42D tub-Gal80 / CyO*. Crosses were performed at 25ºC and 48h AEL larvae were heat-shocked for 1 hour. Wandering L3 larvae were collected, dissected and processed for immunofluorescence analysis.

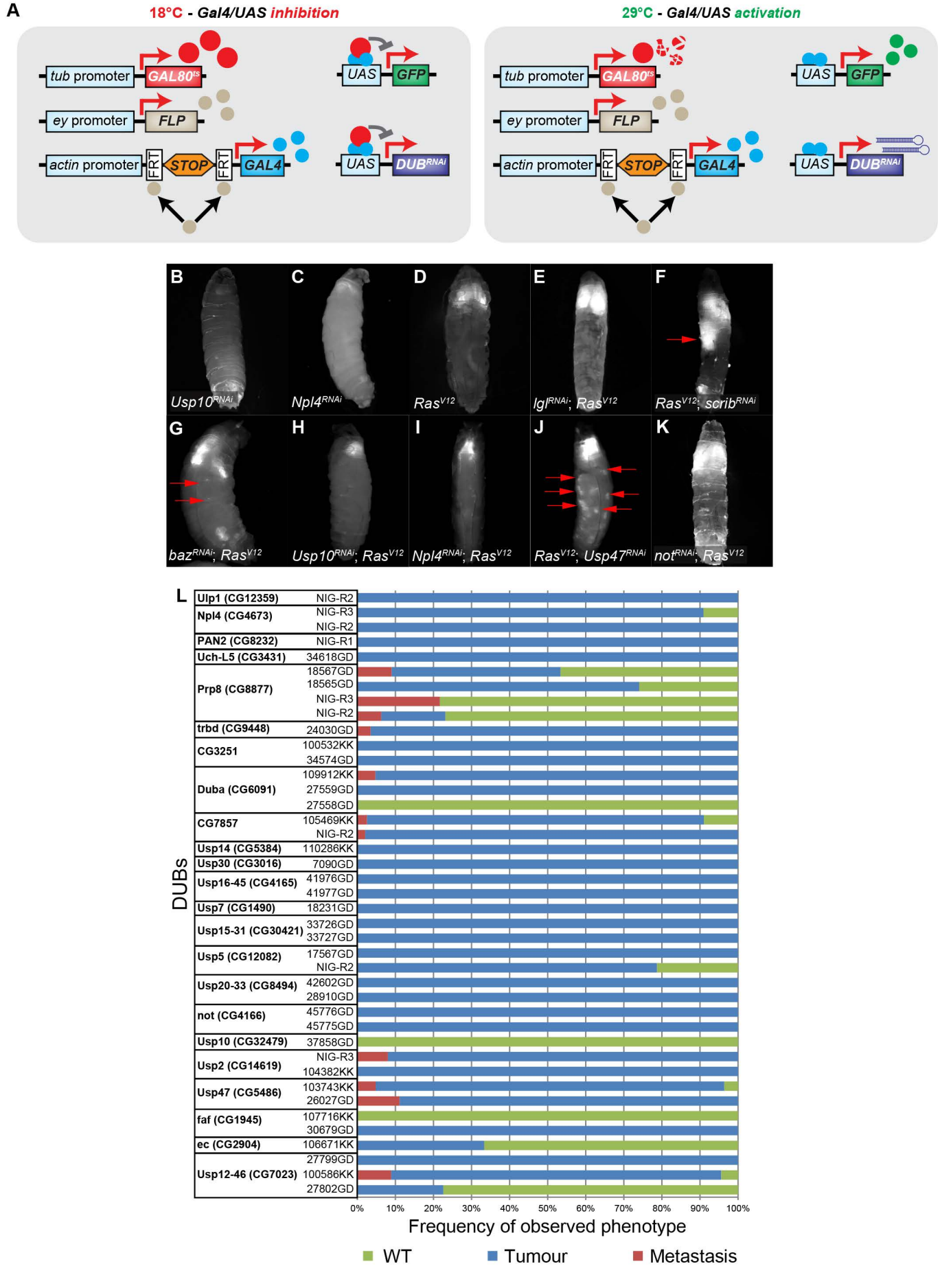
A
18°C - Gal4/UAS inhibition
29°C - Gal4/UAS activation
tub promoter
GAL80ts
ey promoter
FLP
actin promoter
FRT
STOP
FRT
GAL4
UAS
GFP
UAS
DUBRNAi
B
Usp10RNAi
C
Npl4RNAi
D
RasV12
E
lglRNAi; RasV12
F
RasV12; scribRNAi
G
bazRNAi; RasV12
H
Usp10RNAi; RasV12
I
Npl4RNAi; RasV12
J
RasV12; Usp47RNAi
K
notRNAi; RasV12
L
DUBs
Ulp1 (CG12359) NIG-R2
Npl4 (CG4673) NIG-R3
NIG-R2
PAN2 (CG8232) NIG-R1
Uch-L5 (CG3431) 34618GD
Prp8 (CG8877) 18567GD
18565GD
NIG-R3
NIG-R2
trbd (CG9448) 24030GD
CG3251 100532KK
34574GD
Duba (CG6091) 109912KK
27559GD
27558GD
CG7857 105469KK
NIG-R2
Usp14 (CG5384) 110286KK
Usp30 (CG3016) 7090GD
Usp16-45 (CG4165) 41976GD
41977GD
Usp7 (CG1490) 18231GD
Usp15-31 (CG30421) 33726GD
33727GD
Usp5 (CG12082) 17567GD
NIG-R2
Usp20-33 (CG8494) 42602GD
28910GD
not (CG4166) 45776GD
45775GD
Usp10 (CG32479) 37858GD
Usp2 (CG14619) NIG-R3
104382KK
Usp47 (CG5486) 103743KK
26027GD
faf (CG1945) 107716KK
30679GD
ec (CG2904) 106671KK
Usp12-46 (CG7023) 27799GD
100586KK
27802GD
0% 10% 20% 30% 40% 50% 60% 70% 80% 90% 100%
Frequency of observed phenotype
WT
Tumour
Metastasis

Figure S1 – *In vivo* DUB^{RNAi} screen in Ras^{V12} background.

(A) Schematic representation of genetic system controlling the expression of UAS transgenes in the developing eye imaginal disc. Temporal and spatial control of gene expression was achieved by combining *eyFLP* with an *act-Gal4* FLPout cassette and a *tub-Gal80^{ts}* element, such that expression is limited to *ey*-expressing regions upon incubation at 29ºC. **(B-K)** Images of third instar larvae showing distribution of GFP expression induced in the eye discs and optic lobes of the indicated genotypes. Note that (D) is the same representative *Ras^{V12}* larva as depicted in **Fig. 1B**. (B and C) depict other hits from RNAi screen, while (E-G) show screen validation experiments combining *Ras^{V12}* expression with RNAi-mediated depletion of polarity genes. The pattern of GFP distribution in whole larvae shows a variety of phenotypes of proliferation (E) and metastasis (F and G, red arrows). (H-K) are representative images of different phenotypes obtained with selected *DUB^{RNAi}* hits from the screen in combination with expression of *Ras^{V12}*. **(L)** Quantification of phenotype frequency for the indicated genotypes in combination with *Ras^{V12}* expression (n>60 larvae/genotype).

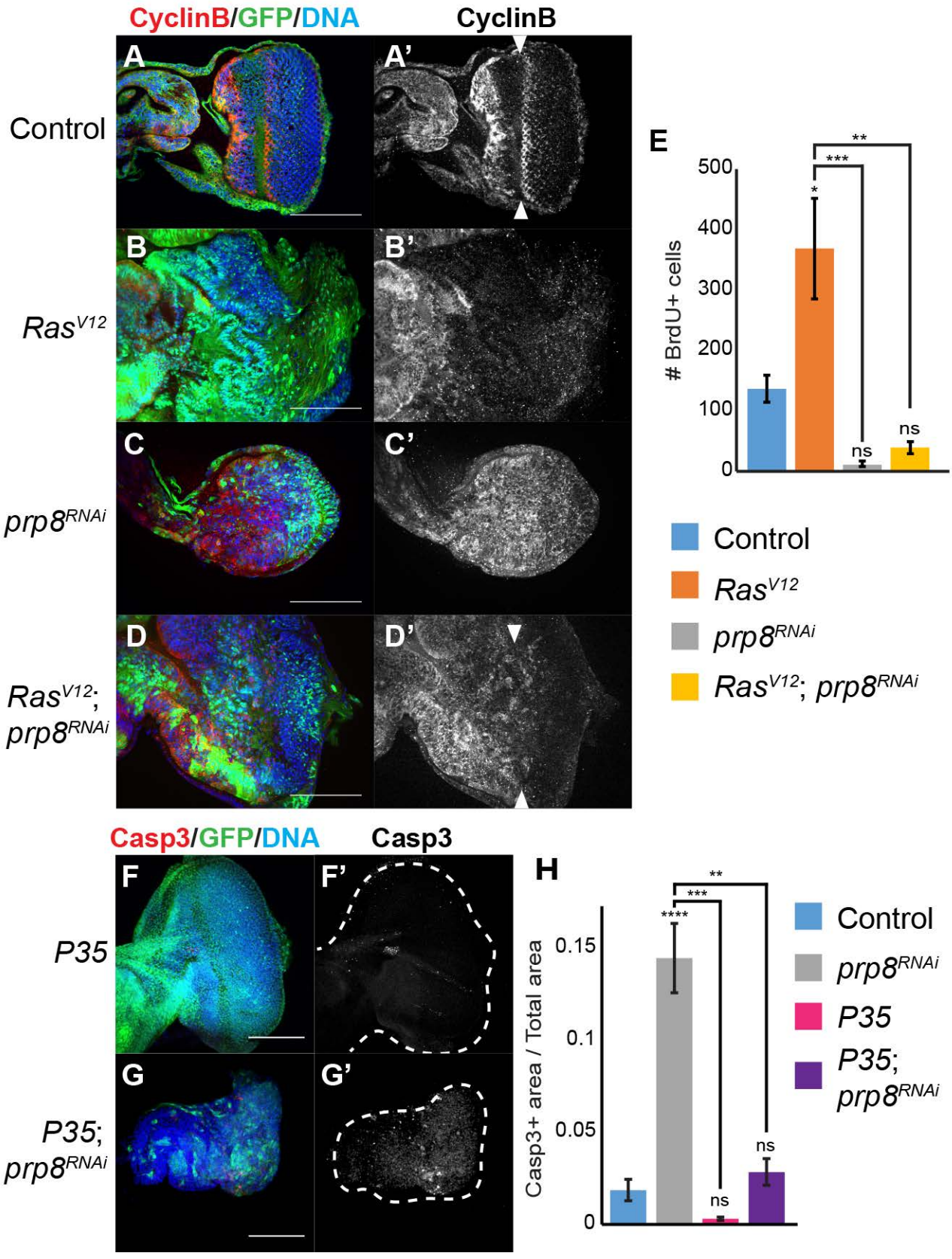

Figure S2 – Analysis of cell proliferation, cell cycle and apoptosis markers in *prp8*^{RNAi}-mediated eye disc hypoplasia.

(A-D) Confocal micrographs of eye imaginal discs of the indicated genotypes, labelled with anti-Cyclin B (red in merged images (A-D) and gray in single-channel images (A'-D')), anti-GFP (green) and the DNA marker Hoechst (blue). **(E)** Quantification of number of BrdU-positive cells (BrdU+) in the indicated genotypes (n>4 discs/genotype). **(F,G)** Confocal micrographs of eye imaginal discs expressing the apoptosis inhibitor P35 alone (F) or in combination with *prp8*^{RNAi} (G), labelled with anti-cleaved Caspase-3 (Dcp1) (red), anti-GFP (green) and the DNA marker Hoechst (blue). Eye discs expressing P35 alone displayed wild-type morphology (F), while expressing P35 in combination with *prp8*^{RNAi} (G) was insufficient to rescue the hypoplasia phenotype (compare also with Fig. 1F and Fig. 2C). Note that eye discs where P35 was expressed in combination with *prp8*^{RNAi} still showed a degree of cell death, which is likely to be caspase-independent (G'). **(H)** Quantification of the ratio between the area of Caspase-3-positive staining and the total eye disc area (n>4 discs/genotype). Note that the control and *prp8*^{RNAi} data are the same as represented in **Fig. 2J**. Scale bars = 100 μm. Data are shown as mean ± SEM. * = p<0.05; ** = p<0.01; *** = p<0.001; **** = p<0.0001.

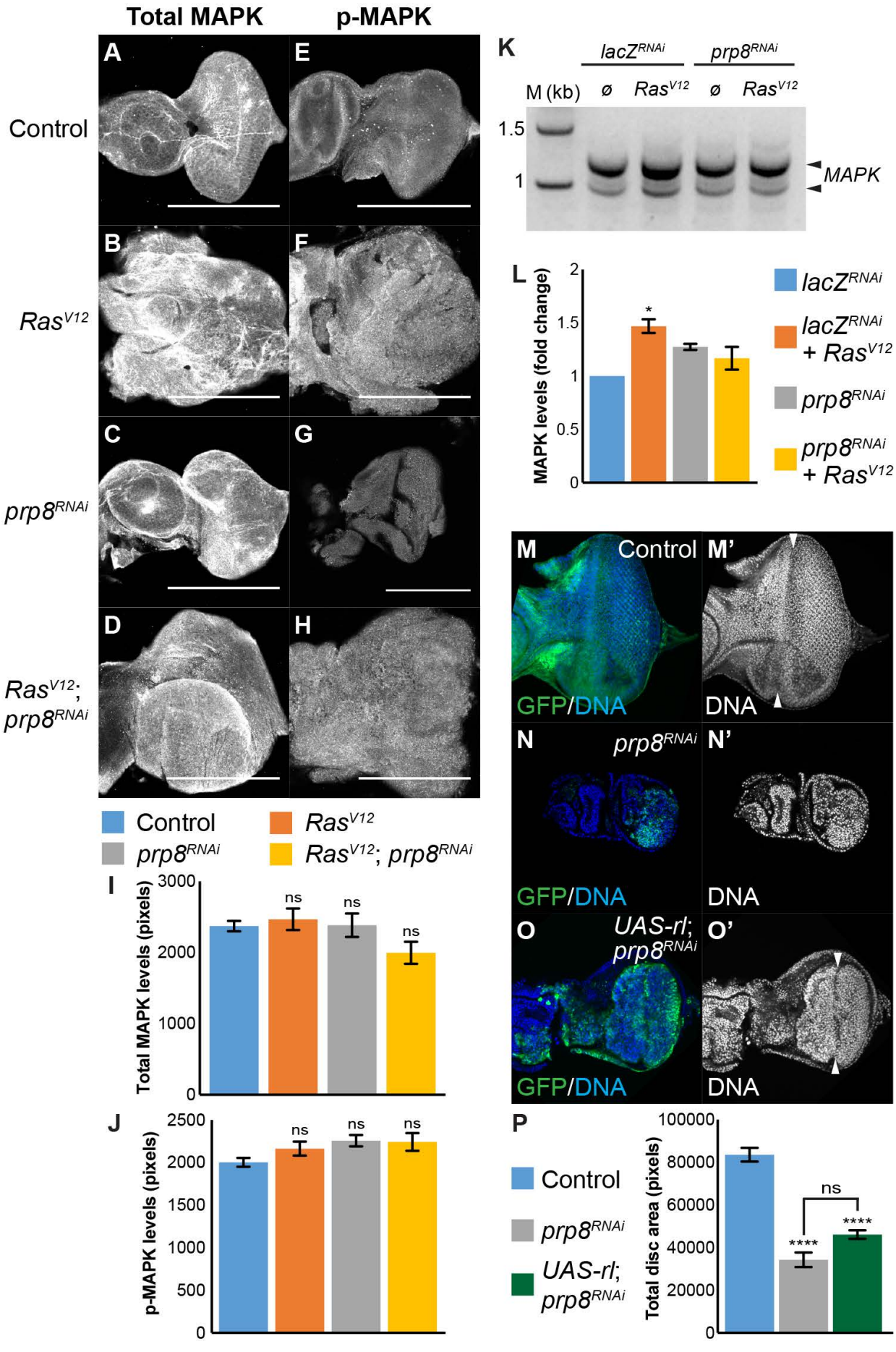

Figure S3 – Effect of *prp8* depletion on MAPK signalling.

(A-H) Confocal micrographs of eye imaginal discs of the indicated genotypes, stained for total MAPK (A-D) or phospho-MAPK (p-MAPK; E-H). **(I)** Quantification of total MAPK levels in eye discs (n>8 discs/genotype). **(J)** Quantification of p-MAPK levels in eye discs (n>5 discs/genotype). **(K)** RT-PCR analysis of MAPK splicing in S2 cells treated with control dsRNA ($lacZ^{RNAi}$) or dsRNA targeting *prp8* ($prp8^{RNAi}$) and transfected with a control plasmid (ø) or Ras^{V12}. **(L)** Quantification of fold change in MAPK expression levels from 2 independent RT-PCR experiments. **(M-O)** Confocal micrographs of eye imaginal discs of the indicated genotypes, stained for GFP (green) and the DNA marker Hoechst (blue (in M-O) or gray (in M'-O'). Arrowheads indicate position of morphogenetic furrow. **(P)** Quantification of eye disc area in the indicated genotypes (n>15 discs/genotype). Expression of MAPK (Rolled; rl) in eye discs depleted of *prp8* (O) is insufficient to suppress the $prp8^{RNAi}$ hypoplasia phenotype (N). Scale bars = 100 μm. Data are shown as mean ± SEM. * = p<0.05; **** = p<0.001. ns = non-significant.

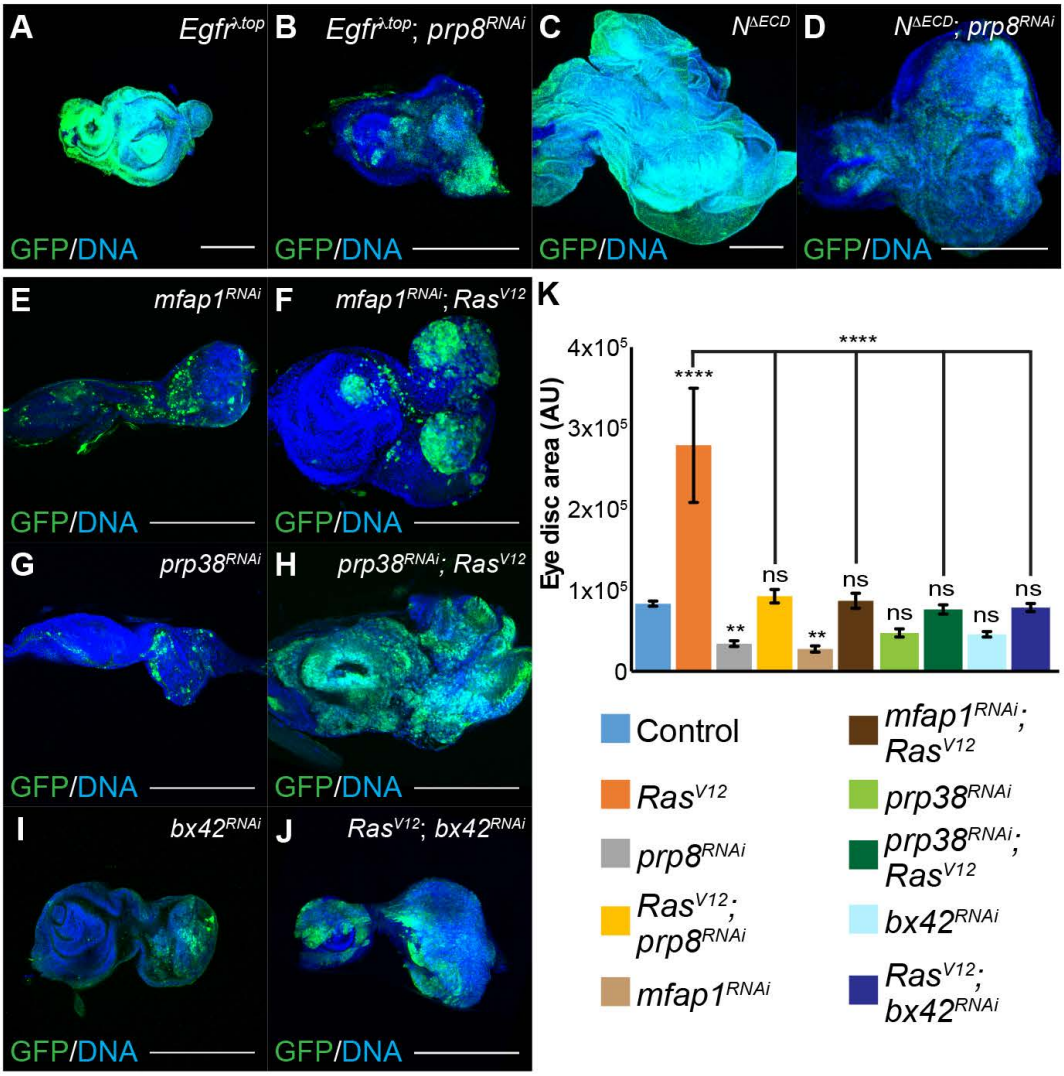

Figure S4 – Effect of RNAi-mediated depletion of spliceosome components on Ras^{V12}-, EGFR- and Notch-induced hyperplastic growth.

(A-D) Confocal micrographs of eye imaginal discs expressing an activated version of the EGF receptor (A; $Egfr^{\lambda top}$), or an activated version of Notch (C; $N^{\Delta ECD}$) alone or in combination with $prp8^{RNAi}$ (B and D, respectively). Eye discs were labelled with anti-GFP (green) and the DNA-binding dye Hoechst (blue). Expression of either oncogene led to hyperplasia (A and C), which was significantly reduced in the presence of $prp8^{RNAi}$. **(E-J)** Confocal micrographs of eye imaginal discs of the indicated genotypes stained with anti-GFP (green) and the DNA marker Hoechst (blue). Note that depletion of spliceosome components in combination with Ras^{V12} expression suppresses the Ras^{V12} hyperplasia phenotype. **(K)** Quantification of eye disc area in the indicated genotypes (n>7 discs/genotype). Scale bar = 200 µm. Data are shown as mean ± SEM. ** = p<0.01; **** = p<0.001. ns = non-significant.

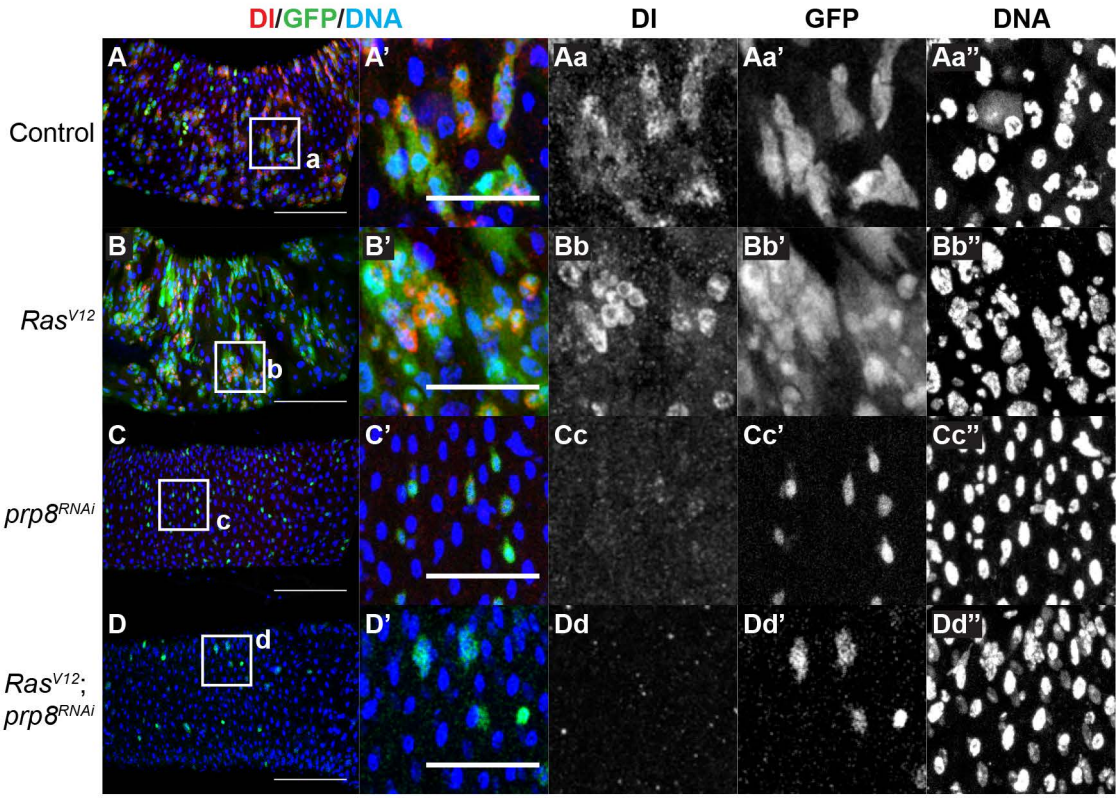

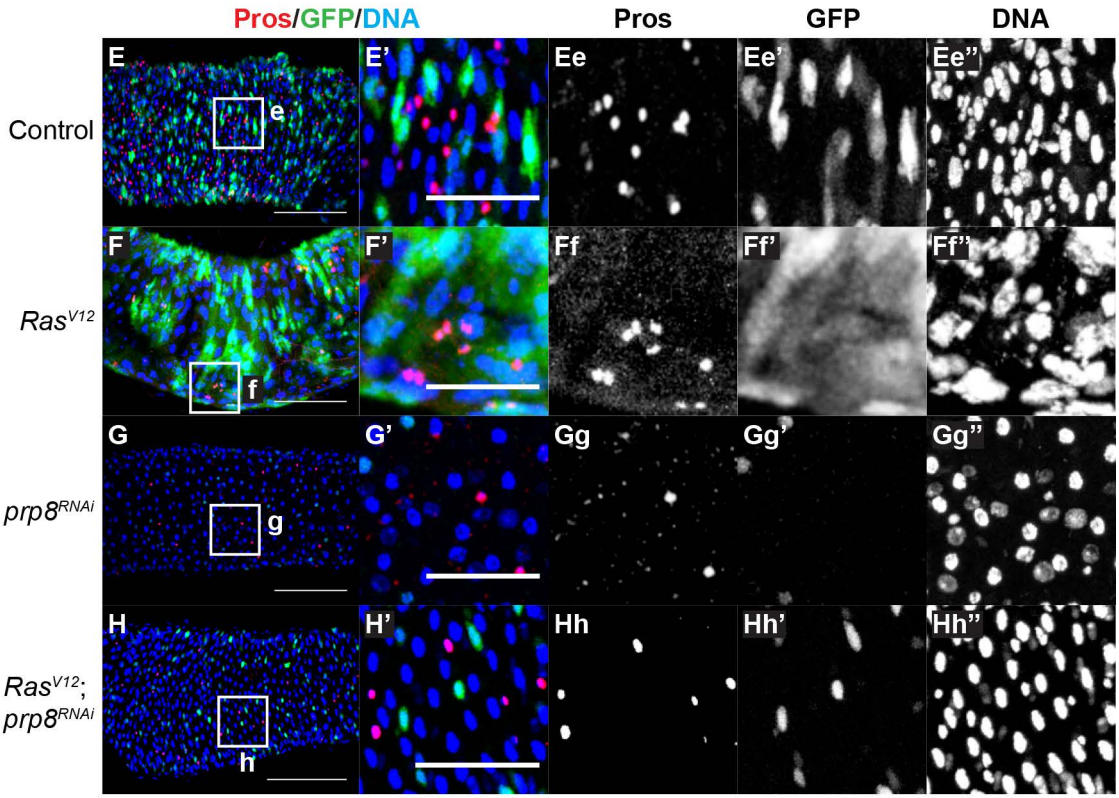

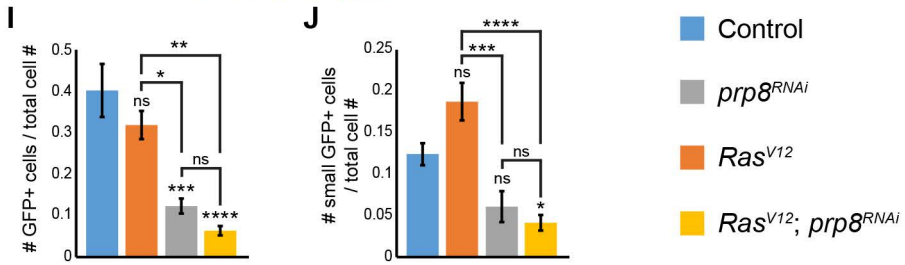

Figure S5 – Prp8 regulates the number of stem cells and enteroendocrine cells in the adult gut.

(A-H) Confocal micrographs of posterior midguts from adult flies of the indicated genotypes, stained for the Notch ligand Delta (Dl, red in A-D) or Prospero (Pros, red in E-H), GFP (green) and DNA (blue). **(a-h)** indicate regions of interest shown in magnified images **(A'-Hh'')**. (A'-H') show merged images, while (Aa-Hh'') depict individual channel images of the magnified region of interest. When compared with controls (A and E), *prp8*^{RNAi} caused a reduction in the number of ISCs, which are both GFP- and Dl-positive (C) and a decrease in the number of enteroendocrine cells, which are marked by Pros expression (G). **(I)** Quantification of the ratio between the number of GPF-positive cells and the total number of cells in the posterior midgut, 7 days after induction (n>9 guts/genotype). **(J)** Quantification of the ratio between the number of small GFP-positive cells (ISCs and progenitors) and the total number of cells in the posterior midgut, 7 days after induction (n>9 guts/genotype). Scale bars = 100 µm (in whole midgut images A-F) and 40 µm (in magnified images). Data are shown as mean ± SEM. * = p<0.05; ** = p<0.01; *** = p<0.001; **** = p<0.0001.

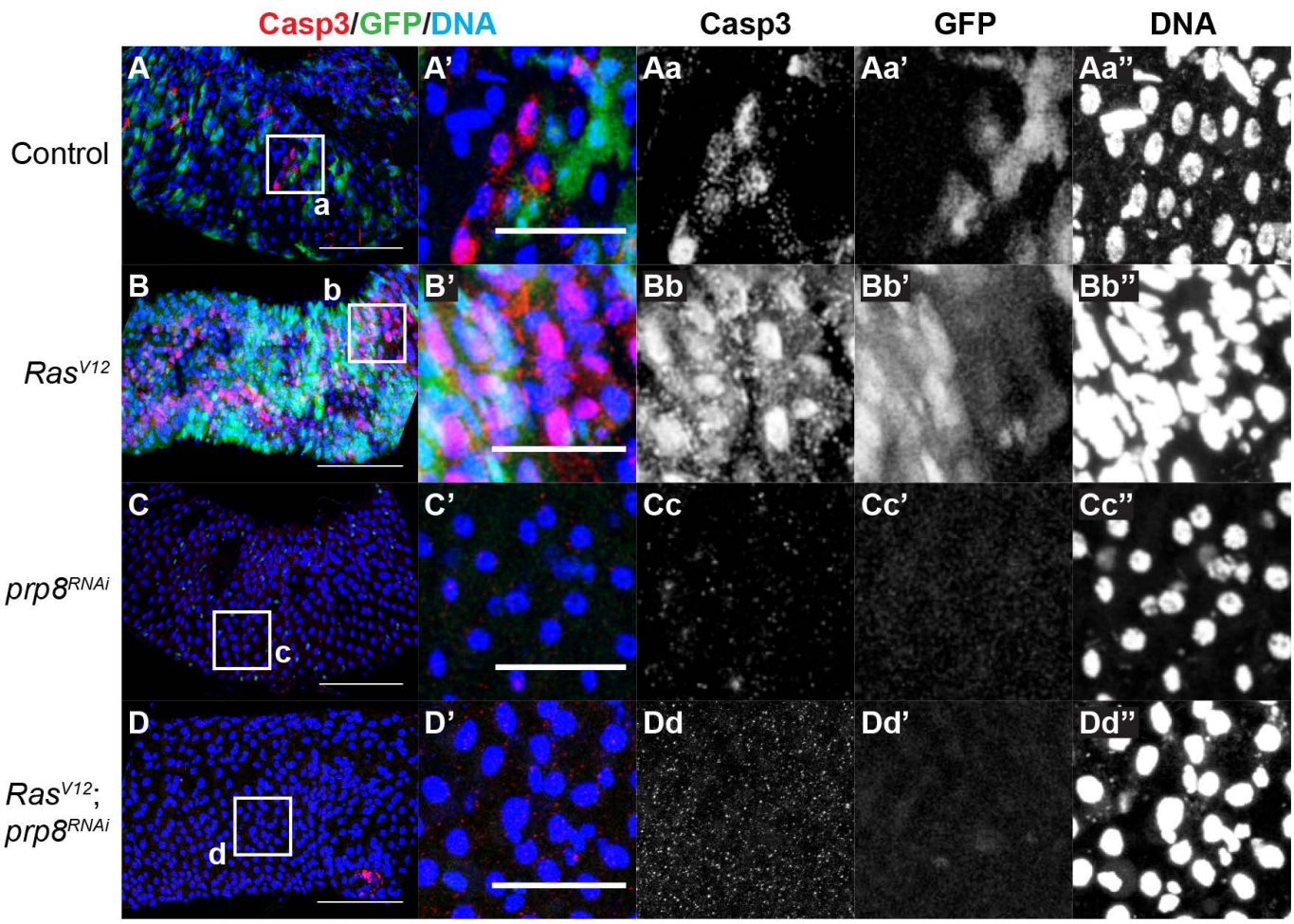

Figure S6 – Prp8 loss is not associated with increased caspase activity in adult guts.

(A-D) Confocal micrographs of posterior midguts from adult flies of the indicated genotypes, stained for activated Caspase-3 (Casp3, red), GFP (green) and DNA (blue) 4 days after transgene induction. **(a-h)** indicate regions of interest shown in magnified images **(A'-Dd'')**. (A'-D') show merged images, while (Aa-Dd'') depict individual channel images of the region of interest. *prp8*^{RNAi} guts displayed reduced levels of activated Caspase-3 (C) when compared with both control (A) and *Ras*^{V12}-expressing flies (B). Scale bars = 100 µm (in whole midgut images A-F) and 40 µm (in magnified images).

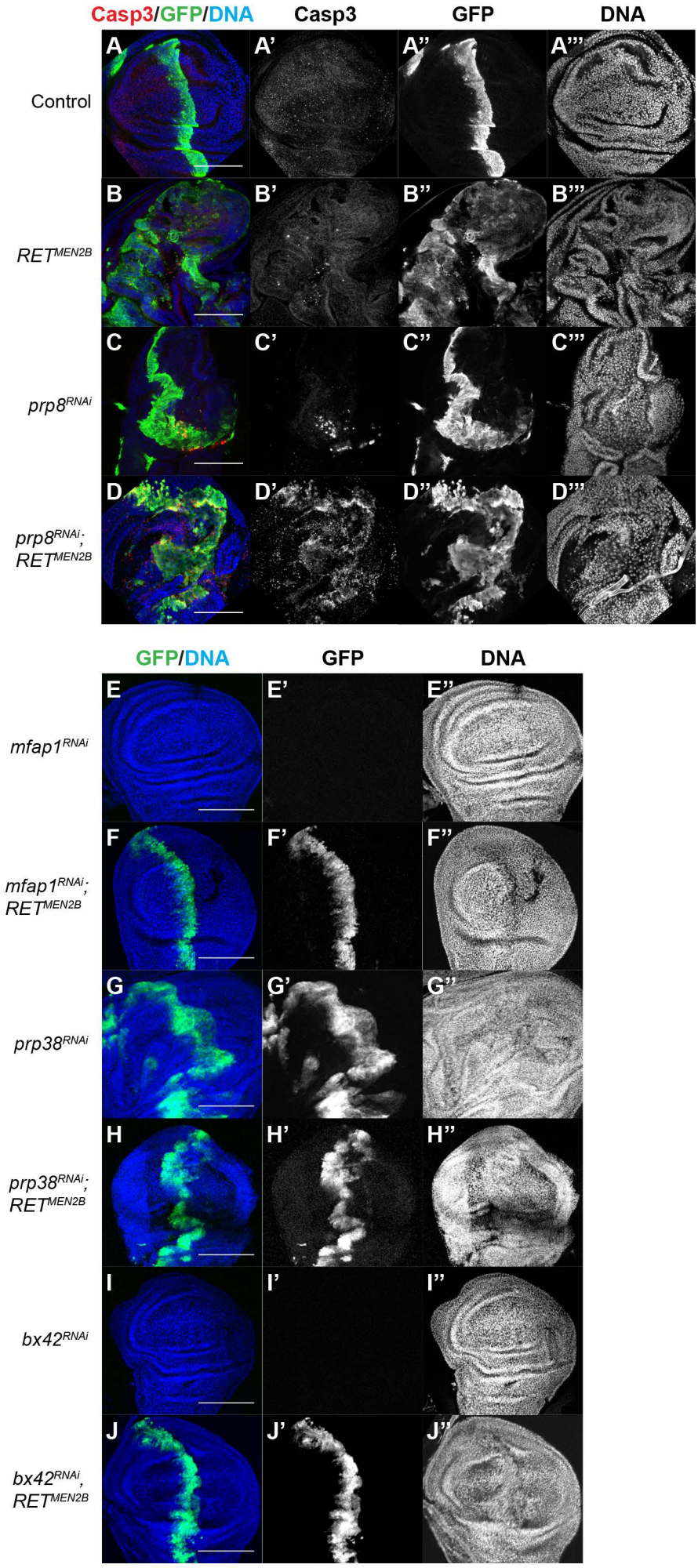

Figure S7 – Caspase activity and effect of depletion of spliceosome components in wing disc tumour model

(A-D) Confocal micrographs of wing imaginal discs from third instar larvae of the indicated genotypes, stained for activated Caspase-3 (Casp3, red), GFP (green) and DNA (blue). GFP expression marks the anterior/posterior boundary and the *ptc-Gal4*-expressing domain. RET^{MEN2B} expression (B) and *prp8* depletion ($prp8^{RNAi}$; C) caused an increase in the GFP-positive area, when compared to controls (A) and, in the case of $prp8^{RNAi}$, this is associated with an increase in the levels of caspase activity (C'). Combining RET^{MEN2B} and $prp8^{RNAi}$ led to enhancement of the RET^{MEN2B} phenotype and the appearance of invasive cells outside the anterior/posterior boundary (D) and a marked increase in the levels of caspase activity (D'). **(E-J)** Confocal micrographs of wing imaginal discs from third instar larvae of the indicated genotypes, stained for GFP (green) and DNA (blue). Note that depleting components of the spliceosome resulted in the suppression of the RET^{MEN2B} phenotype (compare F, H and J with B). Scale bars = 100 µm

Table S1 – List of DUB RNAi lines used in the study

Type	Gene name	CG number	Mammalian Orthologue	RNAi lines
DUB-USP	Usp5	CG12082	USP5, USP13 (IsoT)	CG12082 VDRC 17567 GD CG12082 NIG-FLY 12082-R2 CG12082 NIG-FLY 12082-R1
DUB-USP	Usp2	CG14619	USP2, USP21	CG14619 VDRC 104382 CG14619 NIG-FLY 14619-R1 CG14619 NIG-FLY 14619-R2 CG14619 NIG-FLY 14619-R3
DUB-USP	Usp1	CG15817	USP1	CG15817 VDRC 41604 GD CG15817 VDRC 100992 KK CG15817 VDRC 41605 GD
DUB-USP	Usp30	CG3016	USP30	CG3016 VDRC 7090 GD
DUB-USP	Usp15-31	CG30421	USP31, USP43	CG30421 VDRC 33727 GD CG30421 VDRC 33726 GD CG30421 VDRC 103553 KK
DUB-USP	Usp10	CG32479	USP10	CG32479 VDRC 37858 GD CG32479 VDRC 37859 GD
DUB-USP	Usp16-45	CG4165	USP16, USP45	CG4165 VDRC 41977 GD CG4165 VDRC 110286 KK CG4165 VDRC 41976 GD
DUB-USP	Usp14	CG5384	USP14	CG5384 VDRC 28647 GD CG5384 VDRC 110227 KK CG5384 VDRC 27405 GD
DUB-USP	puf	CG5794	USP34	CG5794 VDRC 27517 GD CG5794 VDRC 106192 KK
DUB-USP	Usp8	CG5798	USP8	CG5798 VDRC 107623 KK
DUB-USP	Usp12-46	CG7023	USP12, USP46	CG7023 VDRC 27802 GD CG7023 VDRC 100586 KK CG7023 VDRC 27799 GD
DUB-USP	Usp32	CG8334	USP6, USP32	CG8334 VDRC 18981 GD CG8334 VDRC 18982 GD
DUB-USP	Usp20-33	CG8494	USP20, USP33	CG8494 VDRC 42609 GD CG8494 VDRC 28910 GD
DUB-USP	DUBAI	CG8830	USP35, USP38	CG8830 VDRC 28960 GD
DUB-USP	CYLD	CG5603	CYLD	CG5603 VDRC 15340 GD CG5603 VDRC 101414 KK
DUB-USP	ec	CG2904	USP53, USP54	CG2904 VDRC 106671 KK CG2904 NIG-FLY 2904-R1
DUB-USP	faf	CG1945	USP9X, USP9Y	CG1945 VDRC 30679 GD CG1945 VDRC 107716 KK
DUB-USP	not	CG4166	USP22, USP27, USP51	CG4166 VDRC 45775 GD CG4166 VDRC 45776 GD
DUB-USP	Usp47	CG5486	USP47	CG5486 VDRC 26027 GD CG5486 VDRC 103743 KK
DUB-USP	scny	CG5505	USP17, USP36, USP42	CG5505 VDRC 105989 KK CG5505 VDRC 11152 GD
DUB-USP	Usp7	CG1490	USP7	CG1490 VDRC 18231 GD CG1490 VDRC 110324 KK
DUB-USP	Usp39	CG7288	USP39 (SNUT2)	CG7288 NIG-FLY 7288-R1 CG7288 VDRC 47663 GD CG7288 VDRC 47664 GD
DUB-USP	PAN2	CG8232	PAN2 (USP52)	CG8232 NIG-FLY 8232R-1
DUB-UCH	Uch	CG4265	UCHL1, UCHL3	CG4265 VDRC 26468 GD CG4265 VDRC 103614 KK
DUB-UCH	Uch-L5	CG3431	UCHL5 (UCH37)	CG3431 VDRC 34618 GD CG3431 VDRC 103481 KK
DUB-UCH	Uch-L5R	CG1950	UCHL5 (UCH37)	CG1950 NIG-FLY 1950R-1
DUB-UCH	calypso	CG8445	BAP1	CG8445 VDRC 47743 GD CG8445 VDRC 107757 KK
DUB-MPN	CG2224	CG2224	STAMBP, STAMBPL, AMSH	CG2224 VDRC 108622 KK CG2224 NIG-FLY 2224-R1 CG2224 NIG-FLY 2224-R3
DUB-MPN	CG4751	CG4751	MPND	CG4751 VDRC 45530 GD
DUB-MPN	CSN5	CG14884	COPS5 (JAB1)	CG14884 NIG-FLY 14884-R1 CG14884 NIG-FLY 14884-R3
DUB-MPN	prp8	CG8877	PRP8	CG8877 VDRC 18565 GD

				CG8877 VDRC 18567 GD CG8877 NIG-FLY 8877-R2 CG8877 NIG-FLY 8877-R3
DUB-MPN	Rpn11	CG18174	PSMD14	CG18174 VDRC 19272 GD
DUB-MPN	Npl4	CG4673	NPLOC4	CG4673 NIG-FLY 4673-R2 CG4673 NIG-FLY 4673-R3 CG4673 VDRC 109309 KK
DUB-MPN	eIF3f2	CG8335	second EIF3F	CG8335 VDRC 15507 GD CG8335 VDRC 108169 KK
DUB-MPN	eIF3f1	CG9769	primary EIF3F	CG9769 VDRC 101465 KK
DUB-MPN	CSN6	CG6932	COPS6	CG6932 VDRC 22308 GD CG6932 VDRC 105385 KK
DUB-MPN	eIF3h	CG9124	EIF3H	CG9124 VDRC 36087 GD
DUB-MPN	Rpn8	CG3416	PSMD7	CG3416 VDRC 26183 GD CG3416 VDRC 108573 KK
DUB-OTU	otu	CG12743	OTUD4 (HIN1)	CG12743 VDRC 47431 GD CG12743 VDRC 108845 KK
DUB-OTU	CG7857	CG7857	OTUD6A / OTUD6B	CG7857 NIG-FLY 7857-R2 CG7857 VDRC 105469 KK
DUB-OTU	CG3251	CG3251	OTUD4 (HIN1)	CG3251 VDRC 34573 GD CG3251 VDRC 34574 GD CG3251 VDRC 100532 KK
DUB-OTU	CG4968	CG4968	OTUB1	CG4968 VDRC 21978 GD
DUB-OTU	CG4603	CG4603	YOD1	CG4603 VDRC 21893 GD CG4603 VDRC 21894 GD
DUB-OTU	Duba	CG6091	OTUD5	CG6091 VDRC 27558 GD CG6091 VDRC 27559 GD CG6091 VDRC 109912 KK
DUB-OTU	trbd	CG9448	ZRANB1 (TRABID)	CG9448 VDRC 24030 GD
DUB-Josph	CG3781	CG3781	JOSD1 / JOSD2	CG3781 VDRC 7113 GD CG3781 VDRC 108379 KK
ULP-SUMO	Ulp1	CG12359	SENP1 / SENP2	CG12359 VDRC 106625 KK CG12359 NIG-FLY 12359-R2 CG12359 NIG-FLY 12359-R4
ULP-SUMO	CG12717	CG12717	SENP6 / SENP7	CG12717 VDRC 106239 KK
ULP-SUMO	CG1503	CG1503	SENP8 (DENP)	CG1503 VDRC 32349 GD CG1503 VDRC 32350 GD CG1503 VDRC 110486 KK
ULP-SUMO	Den1	CG8493	SENP8 (DENP)	CG8493 NIG-FLY 8493-R2 CG8493 VDRC 100591 KK CG8493 VDRC 24110 GD
ULP-SUMO	velo	CG10107	SENP6 / SENP7	CG10107 VDRC 103524 KK
ULP-NEDD8	CG32110	CG32110	SENP1 / SENP2	CG32110 VDRC 107634 KK CG32110 VDRC 34064 GD CG32110 VDRC 34062 GD
DUB-MCPIP	CG10889	CG10889	MCPIP1 (ZC3H12)	CG10889 NIG-FLY 10889-R2 CG10889 NIG-FLY 10889-R3 CG10889 VDRC 27330 GD
DUB-MCPIP	CG42360	CG42360	MCPIP2	CG42360 VDRC 45755 GD CG42360 VDRC 45755 GD

Table S2 – Summary of *in vivo* eye imaginal disc RNAi screen results for major hits

Gene name	RNAi lines	eyGal4 phenotype	Ras screen phenotype
Usp10	CG32479 VDRC 37858 GD	eye disc hypoplasia	tumour reduction
	CG32479 VDRC 37859 GD	wt	ND
prp8	CG8877 VDRC 18565 GD	eye disc hypoplasia	tumour reduction
	CG8877 VDRC 18567 GD	eye disc hypoplasia	tumour reduction/wt
	CG8877 NIG-FLY 8877-R2	eye disc hypoplasia	tumour reduction/wt
	CG8877 NIG-FLY 8877-R3	eye disc hypoplasia	tumour reduction/wt
Npl4	CG4673 NIG-FLY 4673-R2	wt	tumour
	CG4673 NIG-FLY 4673-R3	wt	tumour
	CG4673 VDRC 109309 KK	eye disc hypoplasia	ND

wt: wild-type phenotype; ND: not determined.